MET O 11 TECHNICAL NOTE NO. 186

THE REPRESENTATION OF BOUNDARY LAYER TURBULENCE IN THE MESOSCALE MODEL: PART I - THE SCHEME WITHOUT CHANGES OF STATE

by

R N B Smith

Forecasting Research Branch
Meteorological Office
London Road
Bracknell
Berkshire
RG12 2SZ
United Kingdom

April 1984

1. INTRODUCTION

Over the past decade there have been many "high order turbulence closure" models developed and successfully used to simulate the diurnal evolution of the atmospheric boundary layer (a.b.l.) (e.g. Wyngaard and Coté (1974), Yamada and Mellor (1975), Zeman and Lumley (1976), Oliver et al. (1978), André et al. (1978) and Sun and Ogura (1980)). The order of a closure is determined by which quantities are directly predicted using prognostic equations and which are, on the contrary, parametrized, i.e. expressed with diagnostic equations in terms of the prognostic variables. Thus a 1st-order closure involves predicting ensemble mean variables only and parametrizing all 2nd-order correlations such as the turbulent fluxes.

The models referenced above are all 2nd or higher order and thus cannot strictly be regarded as parametrizations of the turbulent fluxes of heat, moisture and momentum. Their advantage lies in their potential ability to allow for non-local effects, in both space and time, in the turbulence field. A 1st-order closure cannot do this since the fluxes are functions of the local and instantaneous temperature, humidity and velocity fields. However, there is a compromise between the simple 1st-order and the computationally expensive higher-order closures; it is usually called a $1^1/_2$-order scheme. This closure retains only one prognostic 2nd-order turbulence variable, the turbulent kinetic energy (t.k.e.). Models using a prognostic t.k.e. equation are those of Bodin (1979), Yamada and Mellor (1979) and Therry and Lacarrère (1983).

The work of the above authors supports the hypothesis that the important non-localities in the turbulence field can be represented by mean flow advection, turbulent transport and a finite dissipatior rate of t.k.e. All these processes can be included in the t.k.e. equation. The other 2nd-order quantities are expressed in terms of the mean-field variables and the t.k.e. It is known that a detailed representation of a.b.l. structures and processes is required for a correct simulation of many mesoscale features (Anthes (1978)). A representation of boundary layer turbulence using a $1^1/_2$-order closure therefore seems an attractive propostion for

mesoscale models. In addition to providing an improved parametrization of the turbulent fluxes, the formalism also allows diagnosis of consistent values of other 2nd-order quantities. The variances of the three velocity components can be useful parameters when using mesoscale models in pollutant transport studies (Blondin and Therry (1982), Pielke et al. (1982)). The variances and covariances of thermodynamic and water variables are of use in representations of sub-grid scale changes of state.

An alternative approach to this mathematically complicated turbulence closure scheme would be to devise a set of simpler ad hoc parametrizations, one for each type of boundary layer (convective, shear driven, cloud capped etc.) and for the transitions between them. However, such a scheme would not be so easily vectorizable for implementation on the large vector computers now used in NWP. This is because different computations would have to be done at different, temporally varying, sets of grid points. A $1^1/_2$-order closure scheme is, on the contrary, of general applicability (subject to the assumptions of its derivation and implementation) and thus easily vectorized.

This note presents the theoretical derivation of a $1^1/_2$-order turbulence closure, discusses its implementation in a numerical model and presents some results of its use in a one-dimensional and a three-dimensional mesoscale model.

2. THE $1^1/_2$ -ORDER TURBULENCE CLOSURE

2.1 Basic equations for mean variables and turbulent correlations

A basic assumption for all that follows is that the grid point values computed in the numerical model can be identified with ensemble mean values. Deviations from this mean are assumed to be turbulent fluctuations (denoted with a prime). The equations for the ensemble mean model variables ($\underline{v}$, velocity; θ , potential temperature; q, specific humidity) are:

$$\frac{D\underline{v}}{Dt} = -f\,\underline{k}\wedge\underline{v} - g\underline{k} - c_p\theta_v\nabla\pi - \frac{1}{\rho}\frac{\partial}{\partial z}\left(\rho\overline{w'\underline{v}'_h}\right) + \underline{F} \qquad (2.1.1)$$

$$\frac{D\theta}{Dt} = -\frac{1}{\rho}\frac{\partial}{\partial z}\left(\rho\overline{w'\theta'}\right) + \frac{R}{c_p\pi} + F_\theta \qquad (2.1.2)$$

$$\frac{Dq}{Dt} = -\frac{1}{\rho}\frac{\partial}{\partial z}\left(\rho\overline{w'q'}\right) + F_q \qquad (2.1.3)$$

$\theta_v = \theta(1+0.608q)$ is the virtual potential temperature, R is the radiative flux divergence and $\underline{F}$, F_θ , F_q represents the horizontal diffusion terms. In this note changes of state are not considered and so there is no latent heating term in equation (2.1.2) and no source/sink of water vapour in (2.1.3). A companion note will describe the modifications necessary when changes of state occur.

Only vertical derivatives of turbulent correlations are included since these are assumed to dominate in the a.b.l. It is the vertical turbulent fluxes of horizontal momentum, heat and moisture on the r.h.s. of these equations which parametrization schemes seek to represent.

The approach to be developed here is based on a simplification of the equations governing the second and higher order turbulent correlations. It is worth writing these out in full in order to see which terms have to be parametrized or neglected. The equation for the turbulent kinetic energy $\bar{E} = \frac{1}{2}\left(\overline{u'^2} + \overline{v'^2} + \overline{w'^2}\right)$ is

$$\frac{D\bar{E}}{Dt} = -\overline{w'\underline{v}_H'}\cdot\frac{\partial \underline{v}_H}{\partial z} + \frac{g}{\theta_v}\overline{w'\theta_v'} - \frac{1}{\rho}\frac{\partial}{\partial z}\left(\rho\overline{w'E} + \overline{w'p'}\right) - \varepsilon \qquad (2.1.4)$$

The first term on the r.h.s. represents conversion from large scale kinetic energy; the second conversion from large scale potential energy; the third term turbulent transport of t.k.e. including

"pressure transport" and, lastly, ε is the rate of dissipation of t.k.e. The material time derivative on the l.h.s. includes transport of the t.k.e. by the mean flow.

The equations for the remaining second order terms are:

$$\frac{D(\overline{w'\theta'})}{Dt} = -\overline{w'^2}\frac{\partial\theta}{\partial z} + \frac{g}{\theta_v}\overline{\theta_v'\theta'} - \frac{1}{\rho}\frac{\partial}{\partial z}\left(\rho\overline{w'^2\theta'}\right) - P_3^{(\theta)} \qquad (2.1.5)$$

$$\frac{D(\overline{w'q'})}{Dt} = -\overline{w'^2}\frac{\partial q}{\partial z} + \frac{g}{\theta_v}\overline{\theta_v'q'} - \frac{1}{\rho}\frac{\partial}{\partial z}\left(\rho\overline{w'^2q'}\right) - P_3^{(q)} \qquad (2.1.6)$$

$$\frac{D(\overline{\underline{v}_H'\theta'})}{Dt} = -\overline{w'\underline{v}_H'}\frac{\partial\theta}{\partial z} - \overline{w'\theta'}\frac{\partial \underline{v}_H}{\partial z} - \frac{1}{\rho}\frac{\partial}{\partial z}\left(\rho\overline{w'\underline{v}_H'\theta'}\right) - \underline{P}_H^{(\theta)} \qquad (2.1.7)$$

$$\frac{D(\overline{\underline{v}_H'q'})}{Dt} = -\overline{w'\underline{v}_H'}\frac{\partial q}{\partial z} - \overline{w'q'}\frac{\partial \underline{v}_H}{\partial z} - \frac{1}{\rho}\frac{\partial}{\partial z}\left(\rho\overline{w'\underline{v}_H'q'}\right) - \underline{P}_H^{(q)} \qquad (2.1.8)$$

$$\frac{D\,\overline{\theta'^2}}{Dt} = -2\overline{w'\theta'}\frac{\partial\theta}{\partial z} - \frac{1}{\rho}\frac{\partial}{\partial z}\left(\rho\overline{w'\theta'^2}\right) - \varepsilon_\theta \qquad (2.1.9)$$

$$\frac{D\,\overline{q'^2}}{Dt} = -2\overline{w'q'}\frac{\partial q}{\partial z} - \frac{1}{\rho}\frac{\partial}{\partial z}\left(\rho\overline{w'q'^2}\right) - \varepsilon_q \qquad (2.1.10)$$

$$\frac{D(\overline{\theta'q'})}{Dt} = -\overline{w'\theta'}\frac{\partial q}{\partial z} - \overline{w'q'}\frac{\partial\theta}{\partial z} - \frac{1}{\rho}\frac{\partial}{\partial z}\left(\rho\overline{w'\theta'q'}\right) - \varepsilon_{\theta q} \qquad (2.1.11)$$

$$\frac{D(\overline{w'\underline{v}_H'})}{Dt} = -\overline{w'^2}\frac{\partial \underline{v}_H}{\partial z} + \frac{g}{\theta_v}\overline{\underline{v}_H'\theta_v'} - \frac{1}{\rho}\frac{\partial}{\partial z}\left(\rho\overline{w'^2\underline{v}_H'}\right) - \underline{P}_{3H}^{(m)} \qquad (2.1.12)$$

$$\frac{D(\overline{w'^2}-\frac{2}{3}\bar{E})}{Dt} = \frac{2}{3}\left(\overline{w'\underline{v}_H'}\cdot\frac{\partial \underline{v}_H}{\partial z} + 2\frac{g}{\theta_v}\overline{w'\theta_v'}\right) - \frac{1}{\rho}\frac{\partial}{\partial z}\left[\rho\,\overline{w'\left(w'^2-\frac{2}{3}E\right)}\right] - P_{33}^{(m)} \qquad (2.1.13)$$

$$\frac{D(\overline{u'^2}-\frac{2}{3}\bar{E})}{Dt} = \frac{2}{3}\left(-2\overline{w'u'}\frac{\partial u}{\partial z} + \overline{w'v'}\frac{\partial v}{\partial z} - \frac{g}{\theta_v}\overline{w'\theta_v'}\right) - \frac{1}{\rho}\frac{\partial}{\partial z}\left[\rho\,\overline{w'\left(u'^2-\frac{2}{3}E\right)}\right] - P_{11}^{(m)} \qquad (2.1.14)$$

$$\frac{D(\overline{v'^2}-\frac{2}{3}\bar{E})}{Dt} = \frac{2}{3}\left(-2\overline{w'v'}\frac{\partial v}{\partial z} + \overline{w'u'}\frac{\partial u}{\partial z} - \frac{g}{\theta_v}\overline{w'\theta_v'}\right) - \frac{1}{\rho}\frac{\partial}{\partial z}\left[\rho\,\overline{w'\left(v'^2-\frac{2}{3}E\right)}\right] - P_{22}^{(m)} \qquad (2.1.15)$$

In equations (2.1.5) to (2.1.15) there are three types of term which have yet to be specified:

i. The molecular dissipation terms, ε, ε_θ, ε_q and $\varepsilon_{\theta q}$ for t.k.e., potential temperature variance, specific humidity variance and the covariance of potential temperature and specific humidity respectively:

ii. The pressure correlation terms, denoted by the vectors $P_i^{(\theta)}$, $P_i^{(q)}$ and the deviatoric tensor $P_{ij}^{(m)}$; these are defined by

$$P_i^{(\theta)} \equiv \frac{1}{\rho}\overline{\theta'\frac{\partial p'}{\partial x_i}} \quad , \quad P_i^{(q)} \equiv \frac{1}{\rho}\overline{q'\frac{\partial p'}{\partial x_i}} \quad ,$$

$$P_{ij}^{(m)} \equiv \frac{1}{\rho}\left[\overline{v_i'\frac{\partial p'}{\partial x_j}} + \overline{v_j'\frac{\partial p'}{\partial x_i}} - \frac{2}{3}\delta_{ij}\frac{\partial}{\partial x_k}\left(\overline{v_k'p'}\right)\right] \quad ;$$

iii. The third order terms.

2.2 The parametrization of the dissipation and pressure correlation terms

The dissipation terms are parametrized with the aid of the Kolmogorov hypothesis of local, small-scale isotropy. They are given by

$$\varepsilon = \bar{E}/\tau_0 \quad , \quad \varepsilon_\theta = \overline{\theta'^2}/\tau_3 \quad , \quad \varepsilon_q = \overline{q'^2}/\tau_3 \quad , \quad \varepsilon_{\theta q} = (\overline{\theta' q'})/\tau_3$$

where τ_0 and τ_3 are dissipation time scales.

The pressure correlation terms are usually divided into two parts: (i) the part representing the non-linear inertial interactions within the turbulence field which provide the return-to-isotropy mechanism, and (ii) the "rapid" part representing the interactions between the turbulence and mean field quantities such as buoyancy forces and shear. The parametrizations used are:

$$P_i^{(\theta)} = \frac{h_i}{\tau_2} + a_2 \left[-h_k \frac{\partial v_i}{\partial x_k} + \frac{g}{\theta_v} \overline{\theta_v' \theta'} \right] \qquad (2.2.1)$$

$$P_i^{(q)} = \frac{\mu_i}{\tau_2} + a_2 \left[-\mu_k \frac{\partial v_i}{\partial x_k} + \frac{g}{\theta_v} \overline{\theta_v' q'} \right] \qquad (2.2.2)$$

$$P_{ij}^{(m)} = \frac{\pi_{ij}}{\tau_1} + a_1 \left[-\left(\pi_{ik} \frac{\partial v_j}{\partial x_k} + \pi_{jk} \frac{\partial v_i}{\partial x_k} - \frac{2}{3} \delta_{ij} \pi_{kl} \frac{\partial v_k}{\partial x_l} \right) + \left(B_i k_j + B_j k_i - \frac{2}{3} \delta_{ij} B_3 \right) \right] \qquad (2.2.3)$$

where $\pi_{ij} = \overline{v_i' v_j'} - \frac{2}{3} \bar{E} \delta_{ij}$ is the symmetric, traceless Reynolds stress tensor, $h_i = \overline{v_i' \theta'}$ is the heat flux vector, $\mu_i = \overline{v_i' q'}$ is the specific humidity flux vector and $B_i = \frac{g}{\theta_v} \overline{v_i' \theta_v'}$ is the buoyancy flux vector. The first terms, based on the Rotta energy redistribution hypothesis, force the turbulence field back to an isotropic state;

τ_1 and τ_2 are the time scales for this mechanism. The remaining "rapid" terms, involving the non-dimensional constants, a_1 and a_2, are as prescribed by Launder (1975). The value of a_2 is taken to be $1/3$.

The pressure transport term $\overline{w'p'}$ in the t.k.e. equation is neglected or, equivalently, assumed to be proportional to the vertical flux of t.k.e. and hence represented by the choice of constants in the parametrization of this latter term.

2.3 The 1½ -order closure assumptions

Equations (2.1.5) - (2.1.15) can be reduced to purely diagnostic algebraic form by neglecting the material time derivative and the divergences of the third order terms. This simplification of the set of equations is usually called a 1½ -order closure (although Mellor and Yamada (1982) call it a "level 2.5 model"). The only remaining prognostic turbulence variable in this closure is the t.k.e.

With the parametrizations of the dissipation and pressure terms given in § 2.2 and these closure assumptions, equations (2.1.4) - (2.1.15) become:

$$\frac{DE}{Dt} = -\overline{w'\underline{v}_H'}\cdot\frac{\partial \underline{v}_H}{\partial z} + \frac{g}{\theta_v}\overline{w'\theta_v'} - \frac{1}{\rho}\frac{\partial}{\partial z}\left(\rho\overline{w'E}\right) - \frac{\bar{E}}{\tau_o} \qquad (2.3.1)$$

$$\overline{w'\theta'} = \tau_2\left[-\overline{w'^2}\frac{\partial\theta}{\partial z} + (1-a_2)\frac{g}{\theta_v}\overline{\theta_v'\theta'}\right] \qquad (2.3.2)$$

$$\overline{w'q'} = \tau_2\left[-\overline{w'^2}\frac{\partial q}{\partial z} + (1-a_2)\frac{g}{\theta_v}\overline{\theta_v'q'}\right] \qquad (2.3.3)$$

$$\overline{\underline{v}_H'\theta'} = -\tau_2\left[\overline{w'\underline{v}_H'}\frac{\partial\theta}{\partial z} + (1-a_2)\overline{w'\theta'}\frac{\partial \underline{v}_H}{\partial z}\right] \qquad (2.3.4)$$

$$\overline{v_H' q'} = -\tau_2 \left[\overline{w' \underline{v}_H'} \frac{\partial q}{\partial z} + (1-a_2) \overline{w' q'} \frac{\partial \underline{v}_H}{\partial z} \right] \qquad (2.3.5)$$

$$\overline{\theta'^2} = -2 \tau_3 \overline{w' \theta'} \frac{\partial \theta}{\partial z} \qquad (2.3.6)$$

$$\overline{q'^2} = -2 \tau_3 \overline{w' q'} \frac{\partial q}{\partial z} \qquad (2.3.7)$$

$$\overline{\theta' q'} = -\tau_3 \left[\overline{w' \theta'} \frac{\partial q}{\partial z} + \overline{w' q'} \frac{\partial \theta}{\partial z} \right] \qquad (2.3.8)$$

$$\overline{w' \underline{v}_H'} = \tau_1 \left[-\overline{w'^2} \frac{\partial \underline{v}_H}{\partial z} + \frac{g}{\theta_v} \overline{\underline{v}_H' \theta'} \right] \qquad (2.3.9)$$

$$\overline{w'^2} = \frac{2}{3} \bar{E} + \frac{2}{3} \tau_1 \left[\overline{w' \underline{v}_H'} \cdot \frac{\partial \underline{v}_H}{\partial z} + 2 \frac{g}{\theta_v} \overline{w' \theta_v'} \right] \qquad (2.3.10)$$

$$\overline{u'^2} = \frac{2}{3} \bar{E} + \frac{2}{3} \tau_1 \left[-2 \overline{w' u'} \frac{\partial u}{\partial z} + \overline{w' v'} \frac{\partial v}{\partial z} - \frac{g}{\theta_v} \overline{w' \theta_v'} \right] \qquad (2.3.11)$$

$$\overline{v'^2} = \frac{2}{3} \bar{E} + \frac{2}{3} \tau_1 \left[\overline{w' u'} \frac{\partial u}{\partial z} - 2 \overline{w' v'} \frac{\partial v}{\partial z} - \frac{g}{\theta_v} \overline{w' \theta_v'} \right] \qquad (2.3.12)$$

In equations (2.3.9) - (2.3.12) a factor $(1-a_1)$ has been absorbed into the definition of τ_1 thus eliminating the constant a_1. Equations (2.3.2) - (2.3.12), together with the relation

$$\frac{g \theta_v'}{\theta_v} = \frac{g \theta'}{\theta} + \frac{0.608 g q'}{(1 + 0.608 q)} \qquad (2.3.13)$$

form a closed set for the turbulent correlations in terms of the prognostic variables $\underline{v}, \theta, q$ and $\bar{E}$. After much algebraic manipulation the following forms for the vertical turbulent fluxes result:

$$\overline{w'\theta'} = -K_h \frac{\partial \theta}{\partial z} \tag{2.3.14}$$

$$\overline{w'q'} = -K_h \frac{\partial q}{\partial z} \tag{2.3.15}$$

$$\overline{w'\underline{v}_H'} = -K_m \frac{\partial \underline{v}_H}{\partial z} \tag{2.3.16}$$

where the diffusion coefficients are given by:

$$K_h = \frac{\frac{2}{3}\tau_2 \bar{E}}{\left\{1 + 2\tau_2\left[(1-a_2)\tau_3 + \frac{2}{3}\tau_1\right]N^2 + \frac{2}{3}\tau_1^2 S^2 \frac{\left[1+(1-a_2)\tau_2(2\tau_3-\tau_2)N^2\right]}{\left[1+\tau_1\tau_2 N^2\right]}\right\}} \tag{2.3.17}$$

$$K_m = K_h \frac{\frac{\tau_1}{\tau_2}\left[1+(1-a_2)\tau_2(2\tau_3-\tau_2)N^2\right]}{\left[1+\tau_1\tau_2 N^2\right]} \tag{2.3.18}$$

In these formulae the stability parameters S^2 and N^2 are defined by

$$S^2 = S_u^2 + S_v^2 \quad , \quad S_u^2 = \left(\frac{\partial u}{\partial z}\right)^2 \quad , \quad S_v^2 = \left(\frac{\partial v}{\partial z}\right)^2 \tag{2.3.19}$$

$$N^2 = \beta_T \frac{\partial \theta}{\partial z} + \beta_w \frac{\partial q}{\partial z} \quad ; \quad \beta_T = \frac{g}{\theta} \quad , \quad \beta_w = \frac{0.608g}{(1+0.608q)} \tag{2.3.20}$$

The variances of the three velocity components are given by

$$\sigma_w^2 = \frac{2}{3}\left[\bar{E} - \tau_1\left\{K_m S^2 + 2K_h N^2\right\}\right] \qquad (2.3.21)$$

$$\sigma_u^2 = \frac{2}{3}\left[\bar{E} + \tau_1\left\{K_m\left(2S_u^2 - S_v^2\right) + K_h N^2\right\}\right] \qquad (2.3.22)$$

$$\sigma_v^2 = \frac{2}{3}\left[\bar{E} + \tau_1\left\{K_m\left(2S_v^2 - S_u^2\right) + K_h N^2\right\}\right] \qquad (2.3.23)$$

The equations (2.3.14) - (2.3.16) are the familiar flux/gradient relations; these are stated as hypotheses in simpler parametrization schemes. Equation (2.3.14), consistently with (2.3.6), does not allow a counter-gradient heat flux. It is observed that through most of a convectively mixing layer the temperature profile is neutral or even slightly stable in the upper parts below the inversion. The heat flux in such a layer nevertheless remains positive. A closure scheme of this low order cannot represent this. However, a crude but satisfactory way of overcoming this deficiency is to replace (2.3.14) and (2.3.20) by

$$\overline{w'\theta'} = -K_h\left(\frac{\partial\theta}{\partial z} - \gamma_c\right)$$

and $$N^2 = \beta_T\left(\frac{\partial\theta}{\partial z} - \gamma_c\right) + \beta_w\frac{\partial q}{\partial z}$$ respectively,

where γ_c is a slightly stable lapse rate; $\gamma_c = 3 \times 10^{-4}\ ^\circ K\ m^{-1}$ has been used and found to be satisfactory.

2.4 The dissipation and return-to-isotropy time and length scales

All current higher order models and parametrizations assume that the various time scales τ_i are everywhere proportional to each other. Mellor and Yamada (1982) regard this as a deficiency. However, in the absence of any theoretical or experimental work to suggest alternative approaches, and for simplicity, the τ_i are here assumed to be given by $\tau_i = c_i \tau$ where τ is a master time scale and the c_i are non-dimensional constants.

The time scale τ is usually expressed in terms of a basic length scale l:

$$\tau = \frac{l}{\bar{E}^{1/2}} \tag{2.4.1}$$

with l given by the Blackadar formula:

$$\frac{1}{l} = \frac{1}{kz} + \frac{1}{\lambda} \tag{2.4.2}$$

$k = 0.4$ is Von Karman's constant. This prescription for l gives the correct behaviour $l \sim kz$ as $z \to 0$ and gives an asymptotic limit $l \to \lambda$ as $z \to \infty$. There is, however, no dependence on local stability in (2.4.2). André et al. (1978) and Sun and Ogura (1980) introduce some stability dependence in statically stable regions which considerably reduces l there. The latter authors do so by adding a term $N/\bar{E}^{1/2}$ to the r.h.s. of (2.4.2) when $N^2 > 0$. Here a slightly different approach is adopted; in place of (2.4.1) it is assumed that

$$\tau = \frac{l}{(\bar{E} + F_l l^2 N^2)^{1/2}} \tag{2.4.3}$$

with l given by (2.4.2) and F_l a dimensionless constant. This gives $\tau \sim 1/(\sqrt{F_l}\, N)$ as $N^2 \to +\infty$ and $E \to 0$ and reduces to the form (2.4.1) in neutral conditions. Expression (2.4.3) can be written in the form of (2.4.1) as

$$\tau = \frac{l_d}{\bar{E}^{1/2}} \tag{2.4.4}$$

where $l_d = l_d(l, E, N^2)$ is a stability dependent dissipation length given by

$$l_d = \frac{l \bar{E}^{1/2}}{(\bar{E} + F_l l^2 N^2)^{1/2}} \qquad (2.4.5)$$

It can easily be seen that $l_d = l$ in neutral conditions, i.e. the basic length scale given by the Blackadar formula is the neutral dissipation length. Also $l_d \sim \bar{E}^{1/2}/(\sqrt{F_l}\, N)$ as $\bar{E}/N^2 \to 0$ which is the same behaviour as the formulae of André et al. and Sun and Ogura.

Although the expression (2.4.3) is still ad hoc, it has the merit of being a continuous function over the whole stability range. The introduction of another constant F_l might be criticised but, as we shall see in the next section, it gives an extra degree of freedom when choosing the various constants to give the correct critical Richardson number and other empirical constants.

With the τ_i now expressed in terms of the length scale, we can rewrite expressions (2.3.17) and (2.3.18) for K_h and K_m as:

$$K_h = c_o^{-1/3} l_h \bar{E}^{1/2} \qquad (2.4.6)$$

$$K_m = c_o^{-1/3} l_m \bar{E}^{1/2} \qquad (2.4.7)$$

where the stability dependent mixing lengths for heat and momentum, l_h and l_m, are given by

$$l_h = \frac{\frac{2}{3} c_o^{1/3} c_2 \bar{E}^{1/2} (\bar{E} + F_l l^2 N^2)^{1/2} l}{\left\{ \bar{E} + F_3 l^2 N^2 + F_o l^2 S^2 \left[\frac{\bar{E} + F_2 l^2 N^2}{\bar{E} + F_1 l^2 N^2} \right] \right\}} \qquad (2.4.8)$$

$$l_m = l_h \cdot \frac{c_1}{c_2} \frac{(\bar{E} + F_2 l^2 N^2)}{(\bar{E} + F_1 l^2 N^2)} \qquad (2.4.9)$$

The constants in these expressions are defined by

$$F_0 = \tfrac{2}{3} c_1^2 \ , \quad F_1 = c_1 c_2 + F_L \ , \quad F_2 = (1-a_2) c_2 (2c_3 - c_2) + F_L \ , \quad F_3 = 2c_2 \left[(1-a_2) c_3 + \tfrac{2}{3} c_1 \right] + F_L .$$

The asymptotic limit λ for L as $z \to \infty$ is taken to be proportional to the depth of the convectively mixed boundary layer when this exists but not allowed to fall below 40m, i.e.

$$\lambda = \max (40, \alpha h) \tag{2.4.10}$$

where h is the b.l. depth. $\alpha = 1/6$ has been found to give the best results. h is determined from the potential temperature profile; it is taken to be the value of z where a line of gradient $0.35\,^{\circ}K\ km^{-1}$ passing through the value of θ at the bottom model level crosses the profile (see Figure 1).

2.5 The determination of the empirical constants

The constants so far introduced c_0, c_1, c_2, c_3 and F_L can be determined from experimental and observational data. Most of this data is from the surface layer of the atmosphere or near-wall regions in laboratory experiments. In these regions it can fairly accurately be assumed that turbulent energy production is locally balanced by dissipation. Under these conditions equation (2.3.1) for the t.k.e. reduces to diagnostic form. This diagnostic equation for the equilibrium t.k.e. is the quadratic:

$$\bar{E}^2 + \left[(F_1 + F_3 + \tfrac{2}{3} c_0 c_2) l^2 N^2 + \tfrac{2}{3} c_1 (c_1 - c_0) l^2 S^2 \right] \bar{E}$$

$$+ \left[F_1 (F_3 + \tfrac{2}{3} c_0 c_2) l^2 N^2 + \tfrac{2}{3} c_1 (c_1 - c_0) F_2 l^2 S^2 \right] l^2 N^2 = 0 \tag{2.5.1}$$

The larger of the two roots should be taken since the smaller has the physically unrealistic property of being negative whenever $Ri = N^2/S^2 > 0$.

In neutral conditions (2.5.1) reduces to

$$\bar{E}^2 + \tfrac{2}{3} c_1 (c_1 - c_0) l^2 S^2 \bar{E} = 0$$

i.e. $\bar{E}=0$ (the smaller, unphysical root)

or $$\bar{E} = \tfrac{2}{3} c_1 (c_0 - c_1) l^2 S^2 \qquad (2.5.2)$$

If (2.5.2) is substituted in (2.4.9) we get

$$l_m^{(neut., eqm.)} = c_0^{4/3} \cdot \tfrac{2}{3} \tfrac{c_1}{c_0} \left(1 - \tfrac{c_1}{c_0}\right) l$$

The Blackadar l is supposed to be the neutral equilibrium mixing length for momentum i.e. $l_m^{(neut., eqm.)} = l$ and so we must have

$$c_0^{-4/3} = \tfrac{2}{3} \tfrac{c_1}{c_0} \left(1 - \tfrac{c_1}{c_0}\right) \qquad (2.5.3)$$

Equation (2.5.2) for the neutral equilibrium t.k.e. can, with the use of (2.5.3), now be written

$$\bar{E}^{(neut., eqm.)} = c_0^{2/3} l^2 S^2 \qquad (2.5.4)$$

Now $u_*^2 = |\overline{w' \underline{v}'_H}| = |K_m| \cdot |S|$ $= l^2 S^2$ in neutral equilibrium conditions so (2.5.4) becomes

$$\bar{E}^{(neut., eqm.)} = c_0^{2/3} u_*^2$$

There are numerous experimental data for the ratio $u_*^2/\bar{E}$ in neutral equilibrium conditions (or related quantities). The data presented in Table 1 of Mellor and Yamada (1982) suggest $c_0^{-2/3} = 0.32$ is realistic (this corresponds to a value of 2.50 for the ratio q/u_* in this table). This immediately gives

$$c_0 = 5.52427$$

and $c_1 = 1.04694$

Also in neutral conditions the turbulent Prandtl number $P_{rt}=K_m/K_h$ is observed to be 1/1.35 (Businger et al (1971)). Using (2.4.9) we deduce that

$$c_2 = 1.35\, c_1 = 1.41337$$

Three of the empirical constants are thus determined from data relating to equilibrium neutral conditions. The remaining two constants c_3 and F_L are obtained by requiring (i) the equilibrium t.k.e. to vanish at a critical Richardson number (Ri_c) and (ii) the turbulent Prandtl number to tend to unity as the t.k.e. tends to zero. From the zeroth order coefficient in equation (2.5.1) it can be deduced that

$$F_1\left(F_3 + \tfrac{2}{3} c_0 c_2\right) Ri_c = c_0^{2/3} F_2 \qquad (2.5.5)$$

Putting $\bar{E}=0$ in (2.4.9) gives

$$P_{rt}\left(\bar{E}\to 0\right) = \frac{c_1}{c_2} \cdot \frac{F_2}{F_1} = 1 \qquad (2.5.6)$$

Using a value of 0.21 for Ri_c (Businger et al (1971)) these two relationships give

$$c_3 = 3.08492$$

and $F_L = 7.09759$

The derived constants F_i are then computed to be $F_0 = 0.730722$, $F_1 = 8.57730$, $F_2 = 11.57936$ and $F_3 = 14.8840$.

2.6 The truncation to first order closure

If the equilibrium t.k.e. given by equation (2.5.1) is substituted into (2.4.6) to (2.4.9) diffusion coefficients K_h and K_m are obtained as functions of L, Ri and $|S|$. This is then a first order turbulence closure. It is instructive to examine the behaviour of these functions and compare them with those empirically derived.

Equation (2.5.1) can be written in the form

$$e^2 + B(Ri)\,e + C(Ri) = 0 \qquad (2.6.1)$$

where $e = \bar{E}/(c_0^{2/3}\, l^2 S^2)$, i.e. the t.k.e normalised by its neutral equilibrium value. In (2.6.1) B and C are given by

$$\left.\begin{aligned} B(Ri) &= c_0^{-2/3}\left(F_1 + F_3 + \tfrac{2}{3}c_0 c_2\right) Ri - 1 \\ C(Ri) &= c_0^{-2/3}\left[c_0^{-2/3}\left(F_3 + \tfrac{2}{3}c_0 c_2\right) Ri - F_2\right] Ri \end{aligned}\right\} \qquad (2.6.2)$$

From (2.6.1)

$$e(Ri) = \tfrac{1}{2}\left[-B(Ri) + \sqrt{B^2(Ri) - 4C(Ri)}\,\right] \qquad (2.6.3)$$

This gives the asymptotic limit:

$$e \sim c_0^{-2/3}\left(F_3 + \tfrac{2}{3}c_0 c_2\right)|Ri| \qquad (2.6.4)$$

$$= \frac{F_2}{F_1}\frac{|Ri|}{Ri_c} = \frac{c_2}{c_1}\frac{|Ri|}{Ri_c} = \frac{1.35}{0.21}|Ri| = 6.43\,|Ri|$$

We also have e(o)=1 and $e \to 0$ as $Ri \to Ri_c$. The function e(Ri) is shown in Figure 2.

The neutral equilibrium value of K_m is easily seen to be $l^2|S|$. Normalising K_m and K_h with $l^2|S|$ gives:

$$k_m \equiv \frac{K_m}{l^2|S|} = \frac{l_m}{l}\cdot\frac{\bar{E}^{1/2}}{c_0^{1/3} l\,|S|} = \ell_m e^{1/2} \quad \text{where} \quad \ell_m = \frac{l_m}{l} \qquad (2.6.5)$$

$$k_h \equiv \frac{K_h}{l^2|S|} = \ell_h e^{1/2} \quad \text{where} \quad \ell_h = \frac{l_h}{l}$$

$\ell_{h,m}$ are mixing lengths normalised with the neutral mixing length for momentum and are given in terms of e and Ri by:

$$\ell_h(e, Ri) = \frac{\frac{2}{3} c_o^{1/3} c_2 e^{1/2} (e + c_o^{-2/3} F_1 Ri)^{1/2}}{\left\{ e + c_o^{-2/3} F_3 Ri + c_o^{-2/3} F_0 \left[\frac{e + c_o^{-2/3} F_2 Ri}{e + c_o^{-2/3} F_1 Ri} \right] \right\}} \qquad (2.6.6)$$

$$\ell_m(e, Ri) = \ell_h \frac{\frac{c_1}{c_2} (e + c_o^{-2/3} F_2 Ri)}{(e + c_o^{-2/3} F_1 Ri)}$$

Both ℓ_h and $\ell_m \longrightarrow 0$ with $\ell_h/\ell_m \rightarrow 1$ as $e \rightarrow 0$. The equilibrium values of these functions can be computed by substitution of e(Ri) given by (2.6.3) into (2.6.6). The resulting functions $\lambda_{m,h}(Ri) \equiv \ell_{m,h}(e(Ri), Ri)$ have the properties:

$$\left.\begin{aligned} &\lambda_{m,h} \longrightarrow 0 \text{ and } \lambda_h/\lambda_m \rightarrow 1 \text{ as } Ri \longrightarrow Ri_c \\ &\lambda_m(0) = 1, \qquad \lambda_h(0) = 1.35 \\ &\lambda_h \sim \left[\left(\frac{c_2}{c_1 Ri} \right) c_o^{-2/3} \left(F_3 + \frac{2}{3} c_o c_2 - F_1 \right) \right]^{1/2} = 5.17 \\ &\lambda_h/\lambda_m \sim \frac{c_2}{c_1} \left(\frac{F_3 + \frac{2}{3} c_o c_2 - F_1}{F_3 + \frac{1}{3} c_o c_2 - F_2} \right) = 1.83 \\ &\lambda_m \sim 2.83 \end{aligned}\right\} \quad (2.6.7) \quad \text{as } Ri \longrightarrow -\infty$$

In a similar way a normalised dissipation length scale ℓ_d can be defined: $\ell_d = l_d/l$. The function $\ell_d(e, Ri)$ is given by

$$\ell_d(e, Ri) = \frac{e^{1/2}}{(e + c_o^{-2/3} F_1 Ri)^{1/2}} \qquad (2.6.8)$$

and the function $\lambda_d(Ri) \equiv \ell_d(e(Ri), Ri)$ has the properties:

$$\lambda_d \longrightarrow 0 \quad \text{as} \quad Ri \longrightarrow Ri_c \qquad (2.6.9)$$

$$\lambda_d(0) = 1$$

and $$\lambda_d \sim \frac{(F_3 + \frac{2}{3}c_0c_2)^{1/2}}{(F_3 + \frac{2}{3}c_0c_2 - F_i)^{1/2}} = 1.24 \quad \text{as} \quad Ri \to -\infty$$

The functions $\lambda_{d,m,h}(Ri)$ are plotted in Figure 3.

The functions $f_{m,h}(Ri) \equiv k_{m,h}(e(Ri), Ri)$ have the properties:

$$\left.\begin{aligned} & f_{m,h} \to 0 \quad \text{as} \quad Ri \to Ri_c \\ & f_m(0) = 1 \;, \quad f_h(0) = 1.35 \\ & \left.\begin{aligned} f_h &\sim 13.11\,|Ri|^{1/2} \\ f_m &\sim 7.18\,|Ri|^{1/2} \end{aligned}\right\} \text{as } Ri \to -\infty \end{aligned}\right\} \quad (2.6.10)$$

These functions are plotted in Figure 4. The asymptotic dependence as $Ri \to -\infty$ is that predicted by free convection theory.

The empirical first order scheme derived by Richards (1980), and used in the operational coarse and fine mesh models (Foreman (1983)), specifies the functions $f_{m,h}(Ri)$ from surface layer data. In unstable regions ($Ri < 0$) the functions used by Richards (1980) are:

$$f_h(Ri) = (1 - 16\,Ri)^{3/4}$$

and $$f_m(Ri) = (1 - 16\,Ri)^{1/2}$$

These are also shown in Figure 4 for comparison.

For a more direct comparison of empirical stability dependence with the first order closure derived here the functions should be cast in Monin-Obukov similarity form. This is done via the relations:

$$\phi_m = k_m^{-1/2} \quad (2.6.11)$$

$$\phi_h = k_m^{1/2} / k_h$$

and $$\zeta = z/L = Ri\, \phi_m^2 / \phi_h$$

The derived functions $\phi_m(\zeta)$ and $\phi_h(\zeta)$ are plotted in Figure 5. The asymptotic limits are

$$\phi_m(\zeta) \sim 0{\cdot}33 |\zeta|^{-1/3} \quad \text{and} \quad \phi_h(\zeta) \sim 0{\cdot}18 |\zeta|^{-1/3} \quad \text{as} \quad \zeta \to -\infty$$

Again, the $|\zeta|^{-1/3}$ dependence as $\zeta \to -\infty$ is in agreement with the theoretical free convection limit. The empirically derived Monin-Obukhov stability functions as given by Businger et al. (1971) are also shown in Figure 5.

The derived $\phi_{m,h}$ have the correct general shape and numerical agreement is very close in the unstable region for ϕ_h . Agreement is not so close in stable regions for both functions and in the unstable region for ϕ_m . The Businger profiles were derived from surface layer data and one would not expect diffusion or third order terms in the t.k.e. budget to be important near the surface. The disagreement of the first order closure with empirical profiles must, therefore, be due to the treatment of the dissipation and pressure correlation terms. Schumann (1977) has shown that the parametrizations specified in § 2.2 for these terms do not satisfy certian "realisability conditions". However, any remedy for these problems would introduce more complication into the scheme and the choice of the additional constants would not be clear.

2.7 The realisability of the 1½ -order closure

The following inequalities involving turbulent fluctuations must hold:

$$\overline{u'^2},\ \overline{v'^2},\ \overline{w'^2},\ \overline{\theta'^2},\ \overline{q'^2} \geq 0$$

$$(\overline{w'u'})^2 \leq (\overline{w'^2})(\overline{u'^2}) \quad , \quad (\overline{w'v'})^2 \leq (\overline{w'^2})(\overline{v'^2}) \quad , \quad (\overline{u'v'}) \leq (\overline{u'^2})(\overline{v'^2})$$

$$(\overline{\theta' q'})^2 \leq (\overline{\theta'^2})(\overline{q'^2})$$

$$(\overline{w'\theta'})^2 \leq (\overline{w'^2})(\overline{\theta'^2}) \quad , \quad (\overline{u'\theta'})^2 \leq (\overline{u'^2})(\overline{\theta'^2}) \quad , \quad (\overline{v'\theta'})^2 \leq (\overline{v'^2})(\overline{\theta'^2})$$

and similarly for quantities involving q'.

The first set state that the variances of the variables must be non-negative and the remaining conditions are the familiar Schwarz inequalities relating covariances and variances. The parametrizations of these second order quantities derived under $1^1/_2$-order closure assumptions must satisfy these inequalitites for the turbulence field to be "realisable". It can be shown that a sufficient condition for these inequalitites to be satisfied is $\bar{E} \geq -F_6 l^2 N^2$ where $F_6 = F_3 + \frac{2}{3} c_1 c_2 = 15.8705$. This condition ensures a fortiori that $K_{h,m}$ are finite and positive.

2.8 The turbulent energy flux

The remaining quantity to be specified in the $1^1/_2$-order closure scheme is the turbulent vertical flux of t.k.e., $\overline{w'E}$, which is required in the t.k.e. equation (2.3.1). A prognostic equation for this third order quantity can be derived; it contains other third order quantities and fourth order terms. The latter can be eliminated by using the quasi-normal approximation (Lumley et al (1978));

$$\overline{\alpha'\beta'\gamma'\delta'} \simeq \overline{\alpha'\beta'}\ \overline{\gamma'\delta'} + \overline{\alpha'\gamma'}\ \overline{\beta'\delta'} + \overline{\alpha'\delta'}\ \overline{\beta'\gamma'}$$

When this is done the equation can be written as

$$\frac{D(\overline{w'E})}{Dt} = -\overline{w'^2 \underline{v}_H'} \cdot \frac{\partial \underline{v}_H}{\partial z} + \frac{g}{\theta_v}\left(\overline{E\theta_v'} + \overline{w'^2\theta_v'}\right) \qquad (2.8.1)$$

$$-\overline{w'^2}\,\frac{\partial(\bar{E} + \overline{w'^2})}{\partial z} - \overline{w'\underline{v}_H'} \cdot \frac{\partial}{\partial z}\left(\overline{w'\underline{v}_H'}\right) + P$$

P is a pressure correlation term parametrized as

$$P = -\frac{\overline{w'E}}{\tau_4} \qquad (2.8.2)$$

To obtain a simple diagnostic expression for $\overline{w'E}$ gradients of wind and momentum fluxes will be ignored as will the material time derivative. Then(2.8.1) reduces to

$$\overline{w'E} = \tau_4 \left\{ -\overline{w'^2} \frac{\partial}{\partial z}\left(\bar{E} + \overline{w'^2}\right) + \frac{g}{\theta_v}\left(\overline{E\theta_v'} + \overline{w'^2\theta_v'}\right) \right\} \qquad (2.8.3)$$

The two terms in this expression are each divided into two parts as suggested by Therry and Lacarrère (1983):

1st term $E = E_1 + E_2$ where

$$E_1 = -3\,\overline{w'^2}\frac{\partial \bar{E}}{\partial z} \quad , \quad E_2 = \overline{w'^2}\frac{\partial}{\partial z}\left(\overline{u'^2} + \overline{v'^2}\right)$$

2nd term $B = B_1 + B_2$ where

$$B_1 = \frac{3}{2}\frac{g}{\theta_v}\overline{w'^2\theta_v'} \quad , \quad B_2 = \frac{g}{2\theta_v}\left(\overline{u'^2\theta_v'} + \overline{v'^2\theta_v'}\right)$$

On the basis of an experimentally determined budget of $\overline{w'E}$ Therry and Lacarrère (1983) find that the terms E_2 and B_2 are relatively small and so may be neglected. Equation (2.8.3) is thus further simplified to

$$\overline{w'E} = 3\tau_4 \left\{ -\overline{w'^2}\frac{\partial \bar{E}}{\partial z} + \frac{1}{2}\frac{g}{\theta_v}\overline{w'^2\theta_v'} \right\} \qquad (2.8.4)$$

This expression for the vertical flux of t.k.e. contains a familiar down-gradient term and a buoyancy term.

In a convectively mixing boundary layer the t.k.e. flux is observed to be positive whereas the vertical gradient of t.k.e. changes sign from positive in the lower to negative in the upper part. A simple down-gradient expression for $\overline{w'E}$ would therefore give an incorrect profile for this quantity and may be expected to transport too little t.k.e. up to the inversion to maintain entrainment. A reasonably good

specification of $\overline{w'E}$ should be used if an accurate t.k.e. profile is also required for wind variance estimates in pollutant transport studies.

The buoyancy term in (2.8.4) may be expected to represent, partly at least, the observed counter-gradient effects in the t.k.e. flux in convective conditions. If the prognostic equations for $\overline{w'^2\theta'}$, $\overline{w'^2q'}$, $\overline{w'\theta'^2}$, $\overline{w'\theta'q'}$, $\overline{w'q'^2}$, $\overline{\theta'^3}$, $\overline{\theta'^2q'}$, $\overline{\theta'q'^2}$, $\overline{q'^3}$ are simplified in the same way as that for $\overline{w'E}$ the following diagnostic equations are obtained:

$$\frac{g}{\theta_v}\overline{w'^2\theta_v'} = 2\tau_6\left\{-\overline{w'^2}g_2 + \frac{g}{\theta_v}\left(\beta_T\overline{w'\theta_v'\theta'} + \beta_w\overline{w'\theta_v'q'}\right) - \frac{g}{\theta_v}\overline{w'\theta_v'}\frac{\partial\bar{E}}{\partial z} - N^2\overline{w'E}\right\} \qquad (2.8.5)$$

where

$$\frac{g}{\theta_v}\theta_v' = \beta_T\theta' + \beta_w q' \ ,$$

$$g_2 = \beta_T\frac{\partial}{\partial z}\left(\overline{w'\theta'}\right) + \beta_w\frac{\partial}{\partial z}\left(\overline{w'q'}\right) \quad , \quad N^2 = \beta_T\frac{\partial\theta}{\partial z} + \beta_w\frac{\partial q}{\partial z} \ ;$$

and $$\frac{g}{\theta_v}\left(\beta_T\overline{w'\theta_v'\theta'} + \beta_w\overline{w'\theta_v'q'}\right) = \beta_T^2\overline{w'\theta'^2} + 2\beta_T\beta_w\overline{w'\theta'q'} + \beta_w^2\overline{w'q'^2}$$

$$= \tau_8\left\{-\overline{w'^2}g_3 + \frac{g}{\theta_v}\left(\beta_T^2\overline{\theta_v'\theta'^2} + 2\beta_T\beta_w\overline{\theta_v'\theta'q'} + \beta_w^2\overline{\theta_v'q'^2}\right) - \frac{2g}{\theta_v}\overline{w'\theta_v'}g_2 - 2N^2\frac{g}{\theta_v}\overline{w'^2\theta_v'}\right\} \qquad (2.8.6)$$

where

$$g_3 = \beta_T^2\frac{\partial\overline{\theta'^2}}{\partial z} + 2\beta_T\beta_w\frac{\partial(\overline{\theta'q'})}{\partial z} + \beta_w^2\frac{\partial\overline{q'^2}}{\partial z} \ ;$$

and $$\frac{g}{\theta_v}\left(\beta_T\overline{\theta_v'\theta'^2} + 2\beta_T\beta_w\overline{\theta_v'\theta'q'} + \beta_w^2\overline{\theta_v'q'^2}\right)$$

$$= \beta_T^3\overline{\theta'^3} + 3\beta_T^2\beta_w\overline{\theta'^2q'} + 3\beta_T\beta_w^2\overline{\theta'q'^2} + \beta_w^3\overline{q'^3}$$

$$= -3\tau_9\left\{\frac{g}{\theta_v}\overline{w'\theta_v'}g_3 + N^2\left(\beta_T^2\overline{w'\theta'^2} + 2\beta_T\beta_w\overline{w'\theta'q'} + \beta_w^2\overline{w'q'^2}\right)\right\} \qquad (2.8.7)$$

Equations (2.8.4) - (2.8.7) form a closed set and after much algebraic manipulations yield the result:

$$\overline{w'E} = -K_E\frac{\partial\bar{E}}{\partial z} - K_2g_2 - K_3g_3 \qquad (2.8.8)$$

where $$K_E = \frac{\tau_4\left[\left(1+\tau_8\tau_9 N^2+4\tau_6\tau_8 N^2\right)\overline{w'^2}+\left(1+\tau_8\tau_9 N^2\right)\tau_6\,\overline{w'B'}\right]}{\left[\left(1+\tau_8\tau_9 N^2\right)\left(1+\tau_4\tau_6 N^2\right)+4\tau_6\tau_8 N^2\right]} \qquad (2.8.9)$$

$$K_2 = \frac{\tau_4\tau_6\left[\left(1+\tau_8\tau_9 N^2\right)\overline{w'^2}+2\tau_8\,\overline{w'B'}\right]}{\left[\left(1+\tau_8\tau_9 N^2\right)\left(1+\tau_4\tau_6 N^2\right)+4\tau_6\tau_8 N^2\right]} \qquad (2.8.10)$$

$$K_3 = \frac{\tau_4\tau_6\tau_8\left[\overline{w'^2}+\tau_9\,\overline{w'B'}\right]}{\left[\left(1+\tau_8\tau_9 N^2\right)\left(1+\tau_4\tau_6 N^2\right)+4\tau_6\tau_8 N^2\right]} \qquad (2.8.11)$$

where $\overline{w'B'} \equiv \frac{g}{\theta_v}\overline{w'\theta_v'} = -K_h N^2$. The factor 3 in (2.8.4) and (2.8.7) has been absorbed into the definitions of τ_4 and τ_9 respectively.

The timescales are all taken to be proportional to the master timescale τ given by (2.4.3). The constant c_4 is chosen so that, in neutral conditions $K_E = K_m$ i.e. $c_4 = c_1$

The remaining constants are $c_6 = c_8 = 0.81\,c_4$ and $c_9 = 3c_8$.

3. NUMERICAL ASPECTS

3.1 The grid and disposition of the variables

The vertical arrangement of the variables is shown in Figure 6. The t.k.e. and the fluxes of the main model variables are staggered with respect to the main variables. The coefficients K_E, K_2 and K_3 are initially calculated at mid-level points since they are functions of quantities there. However, they are required at the main levels in equation (2.8.8). These coefficients are therefore interpolated to the main levels.

The mesoscale model has its main vertical levels at 10, 110, 310, 610, 1010, 1510, 2110, 2810, 3610, 4510, 5510, 6610, 7810, 9110, 10510, 12010 m above ground with its mid levels half way between these. The

one-dimensional model in which the scheme has been tested has main levels at 10, 100, 300, 500, 700, 900, 1100, 1300, 1500, 1700, 2000 m. Because the grid is, in general, non-linear in z, main levels are not half way between mid-levels. Care has to be taken in interpolating to main levels but no corrections have been applied in the vertical finite differencing to take account of this.

3.2 The prevention of negative t.k.e. and violation of the relisability conditions

The numerical solution of the t.k.e. equation can yield negative values for the t.k.e. This physical impossibility is eliminated by setting a lower bound of $10^{-4}m^2s^{-2}$. The diagnostic t.k.e. equation used to calculate level 1 values (see § 4.3) gives unrealistic negative values when $Ri>Ri_c$. In these circumstances a lower bound of $10^{-3}m^2s^{-2}$ is set.

The realisability condition $\bar{E} + F_6 l^2N^2 \geq 0$ (see § 2.7) is enforced throughout the integration. A lower bound of $-0.935\bar{E}/F_6$ is set for l^2N^2. This is slightly stricter than necessary and gives an upper bound on $\ell_h = l_h/l$ of 10.32, i.e. about twice its equilibrium value as $Ri \to -\infty$ (see (2.6.7)). The replacement of l^2N^2 by this lower bound has been found to be necessary only infrequently. More precisely, the circumstances seem from tests to be restricted to the period just after a nocturnal inversion has been eroded and convective eddies are freely and rapidly growing into the neutral layer left by a previous day's mixing. During this process, lasting half an hour or so, the turbulent energy and fluxes are increasing rapidly mainly through transport from below. This implies that the $1^1/_2$-order closure assumptions, i.e. that $\partial(\overline{w'\theta'})/\partial t$ and $\partial(\overline{w'^2\theta'})/\partial z$ etc. are small compared with local source/sink terms, are not very good. Thus it is not so surprising that this realisability "fix" has to be applied in these circumstances.

3.3 Time integration and numerical stability

The substitution of the diffusivity gradient forms (2.3.14) -(2.3.16) for the fluxes in the equations (2.1.1) - (2.1.3) gives diffusion equations for the basic model variables. (They are not purely diffusive - there are other terms which for the purposes of this discussion can be regarded as "forcing" terms). For example the potential temperature equation can be written as:

$$\frac{\partial \theta}{\partial t} = -\frac{\partial}{\partial z}(\overline{w'\theta'}) + Q = -\frac{\partial}{\partial z}\left(K_h \frac{\partial \theta}{\partial z}\right) + Q \qquad (3.3.1)$$

↑ diffusion term ↑ forcing term

It is well known that an explicit integration of this type of equation will be numerically unstable unless the timestep is small enough. Since this can be quite restrictive in regions where K is large and small, an implicit time integration is often employed.

The situation is further complicated in this type of scheme by the fact that K_h is a function of $\partial\theta/\partial z$. Non-linear diffusion equations of this sort and numerical instabilities associated with them have been discussed by Brown and Pandolfo (1982) and Davies (1983). The usual implicit time integration scheme for (3.3.1) is

$$\Delta\theta = Q^t \Delta t + \Delta t \frac{\partial}{\partial z}\left\{K_h^t\left[\alpha \frac{\partial \theta^{t+1}}{\partial z} + (1-\alpha)\frac{\partial \theta^t}{\partial z}\right]\right\} \qquad (3.3.2)$$

$$0 < \alpha \leq 1$$

$$\Rightarrow \quad \Delta\theta - \alpha \Delta t \frac{\partial}{\partial z}\left[K_h^t \frac{\partial(\Delta\theta)}{\partial z}\right] = \Delta t\left\{Q^t + \frac{\partial}{\partial z}\left(K_h^t \frac{\partial \theta^t}{\partial z}\right)\right\} \qquad (3.3.3)$$

However, it has been found that a non-catastrophic numerical instability can manifest itself when (3.3.3) is used. The main feature of the instability is an oscillation in space and time in K and hence in the fluxes. The oscillations seem to average out so that the

profiles of the diffused variables seem reasonable. In fact there is a very small corresponding oscillation in θ. The functional dependence of K on $\partial\theta/\partial z$ can lead to this small oscillation in θ producing a large oscillation in K. The instability is prevented from being explosive by the smoothing of θ by the diffusion.

The damping of this instability is achieved by recognising the dependence "hidden" in K from the start. Writing the flux of θ as the general function of the gradient:

$$\overline{w'\theta'} = F_\theta\left(\frac{\partial\theta}{\partial z}\right)$$

the generalisation of (3.3.2) is

$$\Delta\theta = Q^t\Delta t + \Delta t\,\frac{\partial}{\partial z}\left\{\alpha F_\theta\left(\frac{\partial\theta^{t+1}}{\partial z}\right) + (1-\alpha)F_\theta\left(\frac{\partial\theta^t}{\partial z}\right)\right\} \qquad (3.3.4)$$

Now expanding $F_\theta\left(\partial\theta^{t+1}/\partial z\right)$ as a Taylor series, to first order in $\Delta\theta$,

$$F_\theta\left(\frac{\partial\theta^{t+1}}{\partial z}\right) = F_\theta\left(\frac{\partial\theta^t}{\partial z}\right) + \left.\frac{\partial F_\theta}{\partial\left(\frac{\partial\theta}{\partial z}\right)}\right|^t \frac{\partial(\Delta\theta)}{\partial z}$$

and substituting in (3.3.4) a generalised version of (3.3.3) is found:

$$\Delta\theta - \alpha\Delta t\,\frac{\partial}{\partial z}\left[\tilde{K}_h^{\,t}\,\frac{\partial(\Delta\theta)}{\partial z}\right] = \Delta t\left\{Q^t + \frac{\partial}{\partial z}\left(K_h^{\,t}\,\frac{\partial\theta}{\partial z}\right)\right\} \qquad (3.3.5)$$

where

$$\tilde{K}_h = -\frac{\partial F_\theta}{\partial\left(\frac{\partial\theta}{\partial z}\right)} = K_h + \frac{\partial K_h}{\partial\left(\frac{\partial\theta}{\partial z}\right)}\,\frac{\partial\theta}{\partial z}$$

Only if K_h does not depend on $\partial\theta/\partial z$ does $\tilde{K}h = Kh$.

The quantity K_h is the <u>effective diffusion coefficient</u> for heat. This can be seen by considering the general variable χ whose turbulent flux is given by

$$\overline{w'\chi'} = -K_\chi\,\frac{\partial\chi}{\partial z}$$

The rate of change of χ due to turbulent transport is

$$-\frac{\partial}{\partial z}\left(\overline{w'\chi'}\right) = \frac{\partial}{\partial z}\left(K_h \frac{\partial \chi}{\partial z}\right) = K_\chi \frac{\partial^2 \chi}{\partial z^2} + \frac{\partial K_\chi}{\partial z}\frac{\partial \chi}{\partial z}$$

Now exhibiting the dependence of K_χ on the gradient $\partial\chi/\partial z$ and other variables $\underline{a}$:

$$K_\chi = K_\chi\left(\frac{\partial \chi}{\partial z}, \underline{a}\right)$$

we have

$$\frac{\partial K_\chi}{\partial z} = \frac{\partial K_\chi}{\partial\left(\frac{\partial \chi}{\partial z}\right)}\frac{\partial^2 \chi}{\partial z^2} + \frac{\partial K_\chi}{\partial \underline{a}} \cdot \frac{\partial \underline{a}}{\partial z}$$

$$\therefore -\frac{\partial}{\partial z}\left(\overline{w'\chi'}\right) = \tilde{K}_\chi \frac{\partial^2 \chi}{\partial z^2} + \frac{\partial K_\chi}{\partial \underline{a}} \cdot \frac{\partial \underline{a}}{\partial z}\frac{\partial \chi}{\partial z} \qquad (3.3.6)$$

where

$$\tilde{K}_\chi = K_\chi + \frac{\partial K_\chi}{\partial\left(\frac{\partial \chi}{\partial z}\right)}\frac{\partial \chi}{\partial z} = -\frac{\partial\left(\overline{w'\chi'}\right)}{\partial\left(\frac{\partial \chi}{\partial z}\right)} \qquad (3.3.7)$$

and the second term in (3.3.6) does not include $\partial^2\chi/\partial z^2$, i.e. is not diffusive.

The effective diffusion coefficients for the variables θ, q, u and v can be shown to be respectively:

$$\tilde{K}_h = K_h\left(1 + t_4 l^2 N_T^2\right) \qquad (3.3.8)$$

$$\tilde{K}_q = K_h\left(1 + t_4 l^2 N_q^2\right) \qquad (3.3.9)$$

$$\tilde{K}_u = K_m\left\{\bar{E} + F_3 l^2 N^2 + F_0 l^2\left[\left(\frac{\partial v}{\partial z}\right)^2 - \left(\frac{\partial u}{\partial z}\right)^2\right] t_2\right\}\Big/ t_3 \qquad (3.3.10)$$

$$\tilde{K}_v = K_m\left\{\bar{E} + F_3 l^2 N^2 + F_0 l^2\left[\left(\frac{\partial u}{\partial z}\right)^2 - \left(\frac{\partial v}{\partial z}\right)^2\right] t_2\right\}\Big/ t_3 \qquad (3.3.11)$$

where $N_T^2 = \beta_T \partial\theta/\partial z$, $N_q^2 = \beta_w \partial q/\partial z$

$$t_4 = \frac{\frac{1}{2}F_1}{(\bar{E}+F_1 l^2 N^2)} - \left[F_3 + \frac{(F_2-F_1)F_0 l^2 S^2 \bar{E}}{t_1^2}\right]\Big/ t_3$$

$$t_1 = \bar{E} + F_1 l^2 N^2 \quad , \quad t_2 = (\bar{E} + F_2 l^2 N^2)/t_1 \, ,$$

$$t_3 = \bar{E} + F_3 l^2 N^2 + F_0 l^2 S^2 t_2 .$$

Hassid and Galperin (1983) have pointed out that for analytic as well as numerical stability the effective diffusion coefficients must be non-negative. The diffusivities $K_{h,m}$ are prevented from becoming negative by the imposition of the realisability conditions (see § 2.7). Additional constraints, without physical justification, have to be applied to ensure non-negative effective diffusion coefficients. These are

$$l^2 N_T^2 \leq t_3/F_3 \tag{3.3.12}$$

$$l^2 N_q^2 \leq t_3/F_3 \tag{3.3.13}$$

and $t_0 \leq (\bar{E}+F_3 l^2 N^2)/t_2$ where $t_0 = F_0 l^2 S^2$ (3.3.14)

The vertically discretised version of (3.3.5) has the form

$$\sum_{l=1}^{NZ-1} M_{kl} \Delta\theta_l = \delta\theta_k \qquad k = 1, \ldots, NZ-1$$

where the $\delta\theta_k$ are the explicit increments and the matrix M is tri-diagonal. The inversion of M to obtain the increments $\Delta\theta_k$ is done by Gaussian elimination.

It has been found necessary for numerical stability to treat the source/sink and dissipation terms in the t.k.e. equation in a partially implicit manner. Writing the t.k.e. equation without advection or turbulent transport terms as

$$\frac{\partial \bar{E}}{\partial t} = -G \qquad \text{where} \quad G = \frac{\bar{E}(\bar{E}+F_i l^2 N^2)^{1/2}}{c_o l} + K_h N^2 - K_m S^2$$

then the implicit time integration scheme used is

$$\Delta E = -\Delta t\, G(E^{t+1}) = -\Delta t\, G(E^t) - \Delta t \left.\frac{\partial G}{\partial E}\right|^t \Delta E$$

which gives $$\left[1 + f_E(E^t)\,\Delta t\right]\Delta E = -\Delta t\, G^t \qquad \text{where} \quad f_E = \frac{\partial G}{\partial E}$$

The function f_E is derived in Appendix A.

4. BOUNDARY CONDITIONS

4.1 Upper boundary conditions

At the top model level it is assumed that the turbulent fluxes of momentum heat and moisture have no divergence. There are thus no increments due to turbulent transports in the wind components, potential temperature and specific humidity at the top level. The upper boundary condition for the t.k.e. specifies that there is no turbulent flux of t.k.e. at the top model level, i.e. $(\overline{w'E})_{NZ}=0$.

4.2 The surface fluxes of momentum, heat and moisture

The formalism developed in § 2 for the turbulent fluxes is not used near the surface as it would require very high vertical resolution to give accurate results. However, so long as the model's bottom level lies within the so-called "constant flux layer"(the bottom few tens of metres) then a parametrization of surface fluxes based on Monin-Obukhov similarity theory should be accurate enough. Such a scheme was developed for the mesoscale model by Carpenter (1977 and 1979).

Carpenter's scheme calculates the turbulent fluxes of momentum, heat and moisture in the surface layer using bulk aerodynamic formulae:

$$(\overline{w'\underline{v}_H'})_{surf} = -C_D |\underline{v}_1| \underline{v}_1 \qquad (4.2.1)$$

$$(\overline{w'\theta'})_{surf} = -C_H |\underline{v}_1| (\theta_1 - \theta_{surf}) \qquad (4.2.2)$$

$$(\overline{w'q'})_{surf} = -C_H |\underline{v}_1| \alpha (q_1 - q_{sat}(T_{surf})) \qquad (4.2.3)$$

$$\alpha = 1/(1 + C_H |\underline{v}_1| r_s)$$

$\underline{v}_1$ is the horizontal wind vector at the bottom model level, r_s is the surface resistance to evaporation and C_D, C_H are drag coefficients which depend on the bulk Richardson number of the surface layer and on a surface roughness length. T_{surf} is a prognostic variable for land points in this scheme. It is determined from an energy budget involving net radiation, the sensible and latent heat fluxes into the atmosphere and a heat flux into the ground.

4.3 The flux of t.k.e. from the surface layer

The first level above the surface at which the t.k.e. is calculated from its prognostic equation is level $1+1/2$. A t.k.e. flux divergence is therefore required between levels 1 and 2. The calculation of $(\overline{w'E})_1$ using (2.8.8) - (2.8.11) involves values of N^2, S^2 and $\tilde{E}$ at level 1. the first two quantities are given by

$$N^2 = \left[\frac{g}{\theta_1}\frac{(\theta_1 - \theta_{surf})}{z_1} + \frac{0.608\, g\, \alpha}{(1+0.608 q_1)}\frac{(q_1 - q_{sat}(T_{surf}))}{z_1}\right] f\left(\frac{z_1}{L}\right) \qquad (4.3.1)$$

$$S^2 = \frac{|\underline{v}_1|^2}{z_1^2}\, g\left(\frac{z_1}{L}\right) \qquad (4.3.2)$$

where

$$\frac{z_1}{L} = \frac{k C_H}{C_D^{3/2}} Ri \quad , \quad Ri = \frac{z_1}{|\underline{v}_1|^2}\left[\frac{g}{\theta_1}(\theta_1 - \theta_{surf}) + \frac{0.608\, g\, \alpha (q_1 - q_{sat}(T_{surf}))}{(1+0.608 q_1)}\right]$$

$$f\left(\frac{z_1}{L}\right) = \frac{c_H \phi_h (z_1/L)}{k c_D^{1/2}} \quad , \quad g\left(\frac{z_1}{L}\right) = \frac{c_D \left[\phi_m (z_1/L)\right]^2}{k^2}$$

f and g are complicated functions of the bulk Richardson number Ri and $\log(z_1/z_0)$. They are in principle computable but the present procedure is to replace them by their neutral values

$$f = 1/\log(z_1/z_0) \quad , \quad g = 1/\left[\log(z_1/z_0)\right]^2 \qquad (4.3.3.)$$

Using these values of N^2 and S^2 a t.k.e. is calculated using the diagnostic equation (2.5.1). The length scale appearing in this equation is taken to be $l=0.7kz$. The factor of 0.7 rather than 1 was found to be necessary to give reasonable values for $\bar{E}$, in unstable conditions. This is possibly due to errors introduced by using approximations (4.3.3) in (4.3.1) and (4.3.2).

Consistent values of N^2, S^2 $\bar{E}$, $\overline{w'^2}$ and $\overline{w'\theta_v'}$ at level 1 can thus be calculated and used to find K_E, K_1, K_2. Values of $\overline{\theta'^2}$, $\overline{\theta' q'}$ and $\overline{q'^2}$ at level 1 can also be calculated so that their gradients can be found.

4.4 The initialisation of the t.k.e.

The t.k.e., being a prognostic variable in this scheme, has to be assigned initial values before an integration can proceed. Since turbulent intensity is not measured in a direct manner routinely and also to ensure a t.k.e. field consistent with the temperature, moisture and wind fields, the initial t.k.e. is calculated from the diagnostic equation (2.5.1).

5. TESTS OF THE SCHEME

5.1 Simulation of Wangara day 33 with a 1-d model

Day 33 of the Australian Wangara experiment (Clarke et al. (1971)) is now very well known. Almost all a.b.l. models and parametrizations are tested on the data from this experiment. The choice of this particular day's data for the simulations is due to there being negligible large-scale forcings (e.g. advection and subsidence) and no cloud. Therefore a one-dimensional model containing only the turbulence and surface exchanges scheme should simulate the main features of the b.l. evolution. The two exceptions to this are: (i) the correct simulation of the wind profile, particularly the development of the nocturnal jet, requires an accurate specification of the time - dependent geostrophic wind profile and (ii) the nocturnal temperature inversion is just as much influenced by radiative exchange with the cool ground as by turbulent transport. The tests reported here used a geostrophic wind constant in time and no radiative exchanges, except those in the surface energy budget, have been included.

The simulation results were obtained using initial profiles from observations at 06.00 hrs local time. The one-dimensional model was dry except for the specification of the specific humidity at level 1 for the surface exchanges. A timestep of 120s was used with the vertical grid specified in § 3.1.

The observed and simulated potential temperature profiles during the daytime are shown in Figures 7 and 8 respectively. A well-mixed layer which deepens and heats up during the course of the day is produced by the model. The growth of the layer into the overlying stable air and the rise in the layer's temperature are both underestimated between 15.00 and 18.00 hours local time. This can perhaps be attributed to the fall off of the surface sensible heat flux (predicted by the surface exchanges component of the model) at a rate greater than that deduced from observations during this period (see Figure 9). The evolution of the b.l. depth in the simulation is shown in Figure 10.

No data are available for the t.k.e. and fluxes so direct verification is not possible. An assessment of the profiles of turbulence variables is aided by plotting them in normalised form. Turbulent velocity fluctuations are normalised with the convective velocity scale w_* given by

$$w_* = \left[\frac{g}{\theta_v} \left(\overline{w' \theta_v'} \right)_{surf} . h \right]^{1/3}$$

and potential temperature fluctuations with θ_* defined by

$$\theta_* = \left(\overline{w' \theta'} \right)_{surf} / w_*$$

The height above the surface and mixing lengths are normalised with the boundary layer height, h.

The profiles of the t.k.e. and vertical velocity variance at 13.00 hours local time are shown in Figure 11. The t.k.e. maximum $\bar{E}_{max} \simeq 0.4 w_*^2$ occurs at $z \simeq 0.4h$. This result is comparable with that obtained by Andre et al. (1978) with their 3rd-order closure model. The vertical velocity variance profile is somewhat more peaked than that of the t.k.e. The more rapid decrease for $\overline{w'^2}$ above the height at which it attains its maximum implies that more of the t.k.e. is in the horizontal components in the upper part of the mixing layer. This seems realistic since the buoyant source of the t.k.e. is strongest in the lower b.l. and feeds energy into the vertical component there. As buoyant parcels of air rise they begin to turn over, i.e. their horizontal velocities increase.

The kinematic heat flux and t.k.e. flux profiles are shown in Figure 12. The linear decrease with height of the heat flux (which gives a uniform heating rate in the b.l.) is well simulated. The negative overshoot of the flux near the inversion, the entrainment heat flux, is underestimated by a factor of about 2. Observations indicate that $(\overline{w'\theta'})_{min} \simeq -0.2 (\overline{w'\theta'})_o$ whereas the factor multiplying the surface flux is about -0.08 in the simulation. The t.k.e. flux is positive through most of

the b.l. despite the positive gradient in t.k.e. below z = 0.4h. This is due to the additional terms in expression (2.8.8) for this flux. The height of the peak of the t.k.e. flux profile, where the transport term in the t.k.e. equation changes sign, is higher than André et al. (1978) predict with their model.

Finally the profiles of the mixing length for heat and the dissipation length are shown in Figure 13. The peak $(l_h)_{max} \simeq 0.5h$ at $z \simeq 0.5h$ accords with intuitive conceptions of the mixing length and its variation within a boundary layer. The maximum value of $\bar{E}^{3/2}/\varepsilon$ is 0.7h and agrees with experiment (Therry and Lacarrère's (1983) Figure 5 composites several sets of experimental results).

5.2 Some results from the mesoscale model with the 1½ -order scheme

The scheme as described in this note, but without the use of virtual temperature in buoyancy and stabilty terms, has been used in the mesoscale model since regular trials began in the summer of 1983. Two twelve hour forecasts produced by the model are presented here. Both are for summer days when there was considerable heating of the land by solar radiation.

The first case is a forecast from 06.00Z data on 14/7/83. Figure 19a, for a gridpoint near Manchester, shows that initially there was a low-level nocturnal inversion about 500 m deep overlying which was a neutral layer of the same depth. The development of the low level winds (at 110 m) and the temperature field (at 10 m) can be seen in Figures 14-17. During the course of the day the model produces a land/sea temperature contrast of over 10 degC which results in sea breezes. This is most marked on the south coast of England. Figure 16 shows that by 18.00Z the sea breeze front has penetrated inland as far as the Thames Valley.

Very little cloud was present to shade the ground in this similation and in these conditions the erosion of the nocturnal inversion and the development of a deep convectively mixed boundary layer is expected.

Figure 19a, which is a time-height cross-section of potential temperature for the bottom 2 km of the model, shows that this is what was produced by the model. Figure 19b is the associated cross-section for the t.k.e. The depth of the boundary layer, as judged by the region of significant turbulence intensity reaches 1200 m by 14.00Z. The t.k.e. between 1000 and 1200 m exists within the inversion; here it entrains the potentially warmer free atmospheric air into the mixing layer and in the process is converted into potential energy.

Figure 18 shows that by 18.00Z some convective clouds have developed. When this forecast was run the deep convection parametrization designed for the model had not been included and so all the cloud and their associated circulations appear on the resolved scales of the model. Of particular note is the patch of cloud which has formed near the gridpoint (26,18). This is clearly evident in Figure 19a where the potential temperature at model level 5 (1010 m) rises due to latent heating after 17.00Z. This immediately has the effect of suppressing turbulence. Since the boundary layer turbulence scheme takes no account of changes of state it interprets the positive potential temperature gradient as an indication of static stabiltiy. This is unrealistic as the latent heating in the boundary layer should be enhancing the sub-gridscale turbulent mixing rather than inhibiting it.

In the second case, run from a data time of 06.00Z on 24/7/83, the region of convective clouds and their circulations, again on the model's resolved scales, is far more extensive. Figures 20-26 show the development of the low-level winds and temperature and the regions of cloudiness. The clouds affect the development of the boundary layer structure in two ways, one realistic and one not. Between about 09.00 and 11.00Z cloud above 2 km was formed in the model at the gridpoint chosen for the time-height cross-sections (Figures 27a and b). This reduced the solar radiation reaching the ground. With the source of buoyancy much reduced, the turbulence in the boundary layer can be seen to die away and the erosion of the low-level inversion ceases. The sky clears after 11.00Z and a convective, turbulent boundary layer is re-established.

The very rapid cessation of turbulence at about 14.40Z is, however, due to the formation of cloud in the boundary layer at the model levels 4 and 5 (at 610 and 1010 m respectively). This abrupt cut-off of turbulence is not realistic and shows that a modification of the scheme to allow for changes of state is needed. Part II of note will discuss how this is done.

No systematic study of the performance of the boundary layer scheme in the mesoscale model has yet been done. This awaits the implementation in the model of the modified "wet" scheme. The interaction of the turbulence parametrization with other parts of the model, particularly the deep convection scheme, will have to be assessed.

ACKNOWLEDGEMENTS

I am grateful to Drs. P W White and K M Carpenter, who gave help and encouragement in the initial stages of this work, and to Dr B W Golding whose useful suggestions and patience were a considerable help latterly. The programming and running of the mesoscale model to produce the results in 5.2 were done by N Machin and other members of the mesoscale group in Met O 11.

APPENDIX A. THE DEVIATION OF f_E

Write G as the sum of a dissipation and source/sink term:

$$G = G_D + G_S \quad \text{where} \quad G_D = \frac{\bar{E}\left(\bar{E} + F_L l^2 N^2\right)^{1/2}}{c_0 l}$$

$$G_S = G_{S1}\, G_{S2}$$

$$G_{S1} = \bar{E} \;, \quad G_{S2} = c_0^{-1/3}\left(l_h N^2 - l_m S^2\right)$$

$$\therefore \frac{\partial G}{\partial \bar{E}} = \frac{\partial G_D}{\partial \bar{E}} + G_{S1}\frac{\partial G_{S2}}{\partial \bar{E}} + G_{S2}\frac{\partial G_{S1}}{\partial \bar{E}} \;.$$

Now the last term = $G_S/2\bar{E}$ and can be positive or negative; it is therefore ignored. (It is required that $f_E = \partial G/\partial \bar{E}$ be +ve and inclusion of this term has been found to cause trouble). Taking $\partial G_S/\partial \bar{E} = G_{S1}\partial G_{S2}/\partial \bar{E}$ implies that only the dependence of $K_{h,m}$ on $\bar{E}$ contained in the mixing lengths $l_{h,m}$ is considered for the implicit treatment of the source/sink terms.

Now $$\frac{\partial G_D}{\partial \bar{E}} = f_{ED} = \tau_0\left(1 + \frac{\frac{1}{2}\bar{E}}{\left(\bar{E} + F_L l^2 N^2\right)}\right)$$

Also $$\frac{\partial G_{S2}}{\partial \bar{E}} = \frac{\partial\left(c_0^{-1/3} l_h\right)}{\partial \bar{E}} N^2 - \frac{\partial\left(c_0^{-1/3} l_m\right)}{\partial \bar{E}} S^2$$

$$= c_0^{-1/3} l_h N^2 \frac{\partial \ln\left(c_0^{-1/3} l_h\right)}{\partial \bar{E}} - c_0^{-1/3} l_m S^2 \frac{\partial \ln\left(c_0^{-1/3} l_m\right)}{\partial \bar{E}}$$

Equations (2.4.8) and (2.4.9) can be written as

$$c_0^{-1/3} l_h = \frac{\frac{2}{3} c_2 \bar{E}^{1/2} t_l^{1/2}}{t_3} \;, \quad c_0^{-1/3} l_m = \frac{c_1}{c_2} t_2 l_h$$

where $t_1 = \bar{E} + F_1 l^2 N^2$

$t_3 = \bar{E} + F_3 l^2 N^2 + t_0 t_2$

$t_0 = F_0 l^2 S^2$

$t_2 = (\bar{E} + F_2 l^2 N^2)/(\bar{E} + F_1 l^2 N^2)$

$$\therefore \frac{\partial \ln (c_0^{-1/3} l_h)}{\partial \bar{E}} = \frac{1}{2}\left(\frac{\partial \ln \bar{E}}{\partial \bar{E}} + \frac{\partial \ln t_1}{\partial \bar{E}}\right) - \frac{\partial \ln t_3}{\partial \bar{E}} = \frac{1}{2}\left(\frac{1}{\bar{E}} + \frac{1}{t_1}\right) - \frac{1}{t_3}\frac{\partial t_3}{\partial \bar{E}} \equiv F_h$$

and

$$\frac{\partial \ln (c_0^{-1/3} l_m)}{\partial \bar{E}} = \frac{\partial \ln (c_0^{-1/3} l_h)}{\partial \bar{E}} + \frac{\partial \ln t_2}{\partial \bar{E}} = F_h + \frac{1}{t_2}\frac{\partial t_2}{\partial \bar{E}} \equiv F_m$$

$$\therefore f_{ES} = G_{S1}\frac{\partial G_{S2}}{\partial \bar{E}} = F_h K_h N^2 - F_m K_m S^2$$

From the definitions of t_2 and t_3:

$$\frac{\partial t_2}{\partial \bar{E}} = \frac{F_4 l^2 N^2}{t_1^2} \quad \text{where} \quad t_1 = \bar{E} + F_1 l^2 N^2 \quad \text{and} \quad F_4 = F_1 - F_2$$

and

$$\frac{\partial t_3}{\partial \bar{E}} = 1 + t_0 \frac{\partial t_2}{\partial \bar{E}} .$$

The required function f_E is then given by

$$f_E = f_{ED} + f_{ES}$$

REFERENCES

André, J.C., de Moor, G., Laccarrère, P., Therry, G. and du Vachat, R. (1978).

Modelling the 24-hour evolution of the mean and turbulent structures of the a.b.l. J. Atmos. Sci. 35, 1861.

Anthes, R.A. (1978).

Boundary layers in numerical weather prediction. Workshop on the P.B.L. Amer. Met. Soc., Boston.

Blondin, C. and Therry, G. (1982).

Preliminary tests of the introduction of Lagrangian modelling in a 3-D atmospheric mesoscale model. Procedings of the 13th. I.T.M. on Air Pollution Modelling and its Applications. Ile des Embiez, France.

Bodin, S. (1979).

A predictive numerical model of the a.b.l. based on the turbulent energy equation. SHMI Report No. 13.

Brown, P.S. and Pandolfo, J.P. (1982).

A numerical predictability problem in the solution of the non-linear diffusion equation. Mon. Weather Rev. 110, 1214.

Businger, J.A., Wyngaard, J.C., Jzumi, Y. and Bradley, E.F. (1971).

Flux-profile relationships in the atmospheric surface layer. J. Atmos. Sci. 28, 181-189.

Carpenter, K.M. (1977).

Surface exchanges in a mesoscale model of the atmosphere. Met O 11 Technical Note No. 96.

Carpenter, K.M. (1979).

An experimental forecast using a non-hydrostatic mesoscale model. Q.J. Royal Met. Soc. 105, 629-655.

Clarke, R.H., Dyer, A.J., Brook, R.R., Reid, D.G. and Troop, A.J. (1971).
The Wangara experiment: Boundary layer data. Technical Paper 19, Div. Met. Phys. CSIRO, Australia.

Davies, H.C. (1983).
The stability of some p.b.l. diffusion equations (1983) Mon. Weather Rev. 111, 2140-2143.

Foreman, S.J. (1983).
The numerical weather prediction model of the UK Meteorological Office. Procedings of the 6th conference on N.W.P., Omaha, Nebraska, June 6-9, 1983 pp 96-101, Amer. Met. Soc.

Hassid, S. and Galperin, B. (1983).
A turbulent energy model for geophysical flows. Boundary Layer Met. 26, 397-412.

Launder, B.E. (1975).
On the effects of a gravitational field on the turbulent transport of heat and momentum. J. Fluid Mech. 67, 569.

Lumley, J.L., Zeman, O. and Siess, J. (1978).
The influence of buoyancy on turbulent transport. J. Fluid Mech. 84, 581.

Mellor, G.L. and Yamada, T. (1982).
Development of a turbulence closure model for geophysical fluid problems. Rev. Geophysics and Space Physics 20, 851-875.

Oliver, D.A., Lewellen, W.S. and Williamson, G.G. (1978).
The interaction between turbulent and radiative transport in the development of fog and low-level stratus. J. Atmos. Sci. 35, 301.

Pielke, R.A., McNider, R.T., Martin, C.L. and Segal, M. (1982).
Thermally driven effects and the parametrization of boundary layer diffusion. Procedings of the workshop on the parametrization of mixed layer diffusion, 20-23 October 1981. Ed. Cionco R.M. Physical Science Lab. New Mexico State Univ. Las Cruces, New Mexico, USA.

Richards, P.J.R. (1980).
The parametrization of boundary layer processes in general circulation models. Ph. D. Thesis. Univ. of Reading, UK.

Schumann, U. (1977).
Realizability of Reynolds-stress turbulence models. Phys. fluids 20, 721-725.

Sun, W.-Y. and Ogura, Y. (1980).
Modelling the evolution of the convective p.b.l. J. Atmos. Sci. 27, 1558.

Therry, G. and Lacarrère, P. (1983).
Improving the eddy kinetic energy model for p.b.l. description. Boundary Layer Met. 25, 63.

Wyngaard, J.C. and Cote, O.R. (1974).
Evolution of a convective p.b.l. - a higher order closure model study. Boundary Layer Met. 7, 289.

Yamada, T. and Mellor, G.L. (1975).
A simulation of the Wangara a.b.l. data. J. Atmos. Sci. 32, 2309.

Yamada, T. and Mellor, G.L. (1979).
A numerical simulation of BOMEX data using a turbulence closure model coupled with ensemble cloud relations. Quart, J. Royal Met. Soc. 105, 915.

Zeman, O. and Lumley, J.L. (1976).
Modelling buoyancy driven mixed layers. J. Atmos. Sci. 33, 1974.

FIGURE 1.

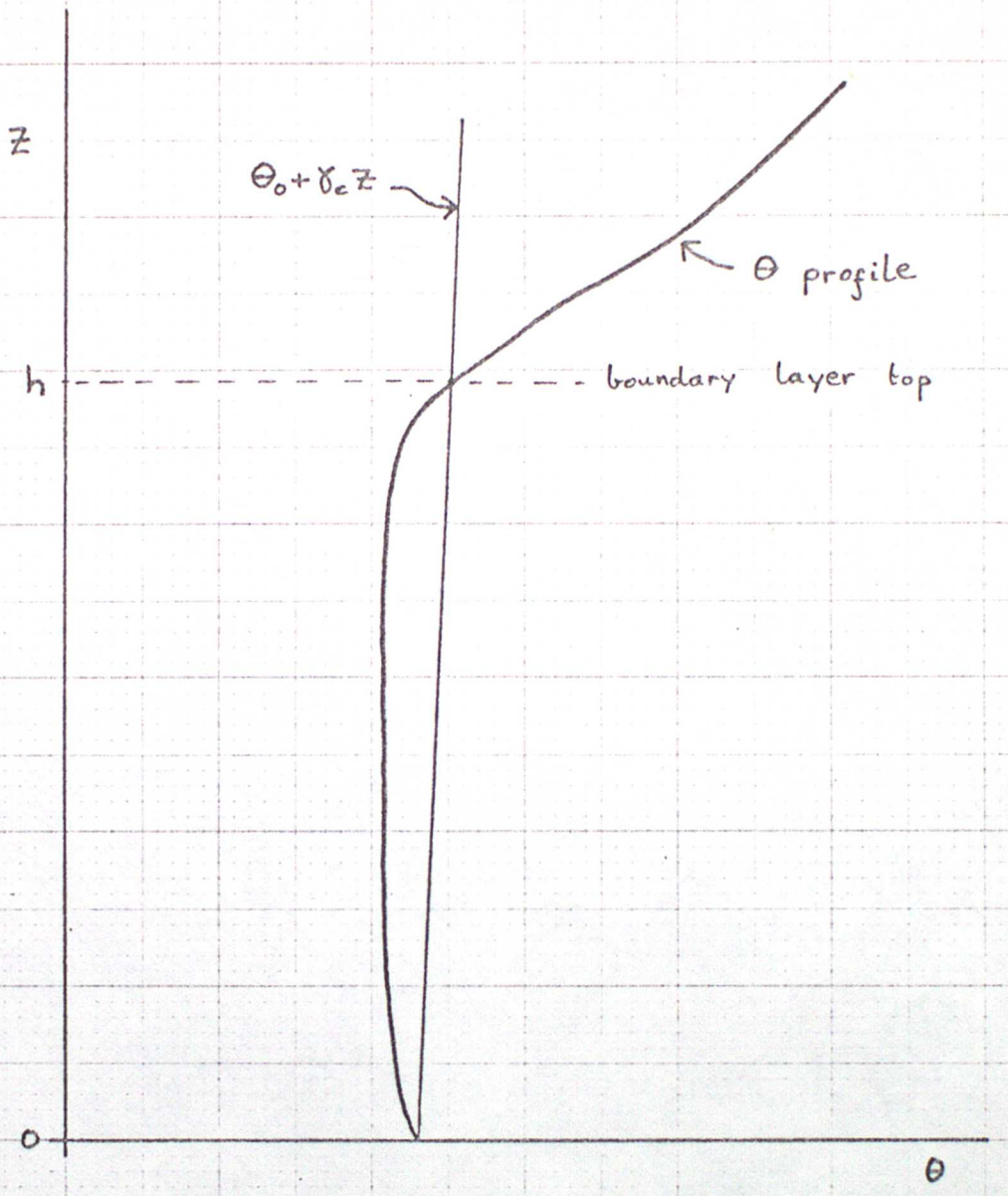

The determination of the boundary layer depth.

FIGURE 2.

NORMALISED EQUILIBRIUM T.K.E. AS A FUNCTION OF THE RICHARDSON NUMBER.

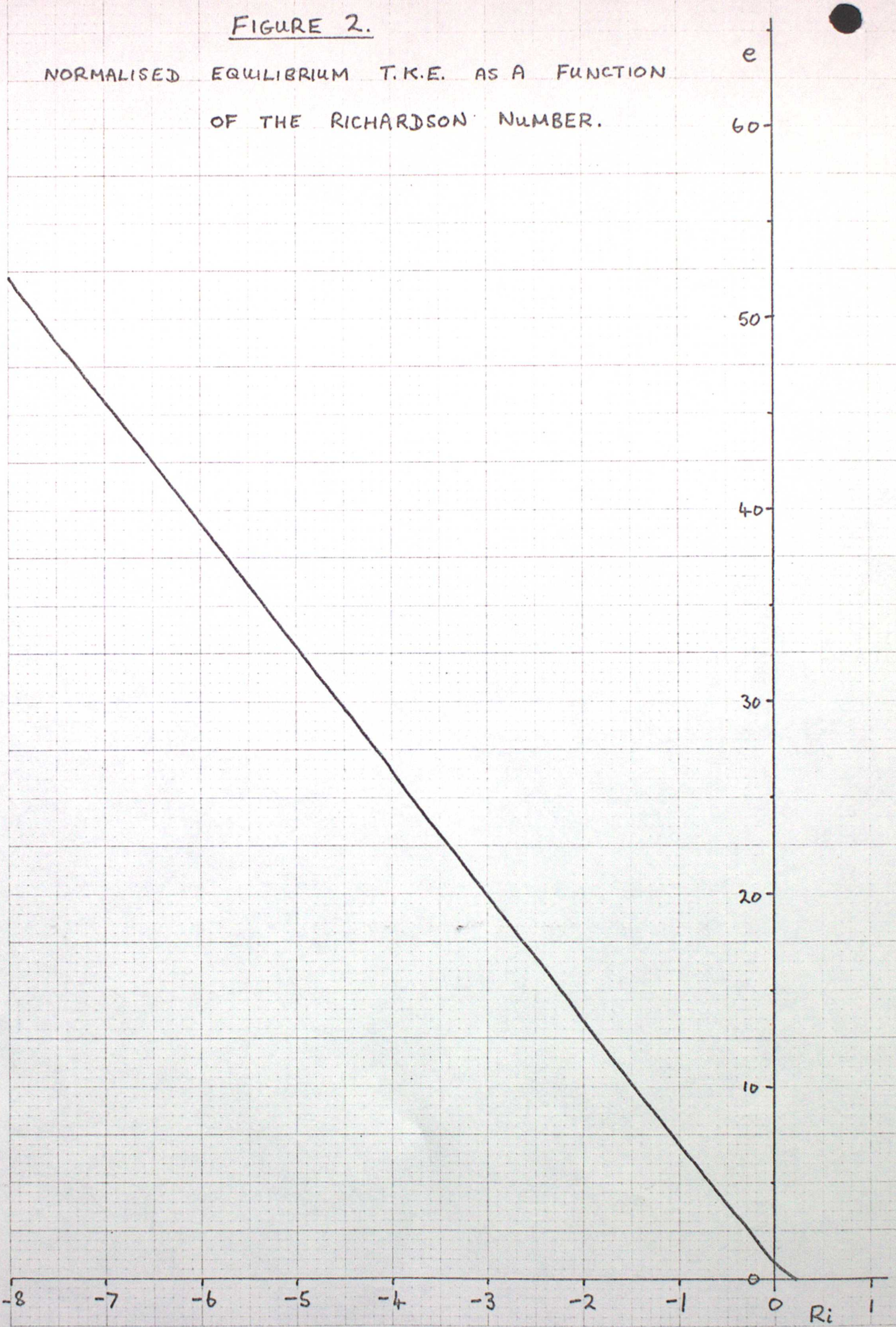

E.R.

FIGURE 3.

NORMALISED MIXING AND DISSIPATION LENGTHS DERIVED FROM FIRST ORDER TRUNCATION.

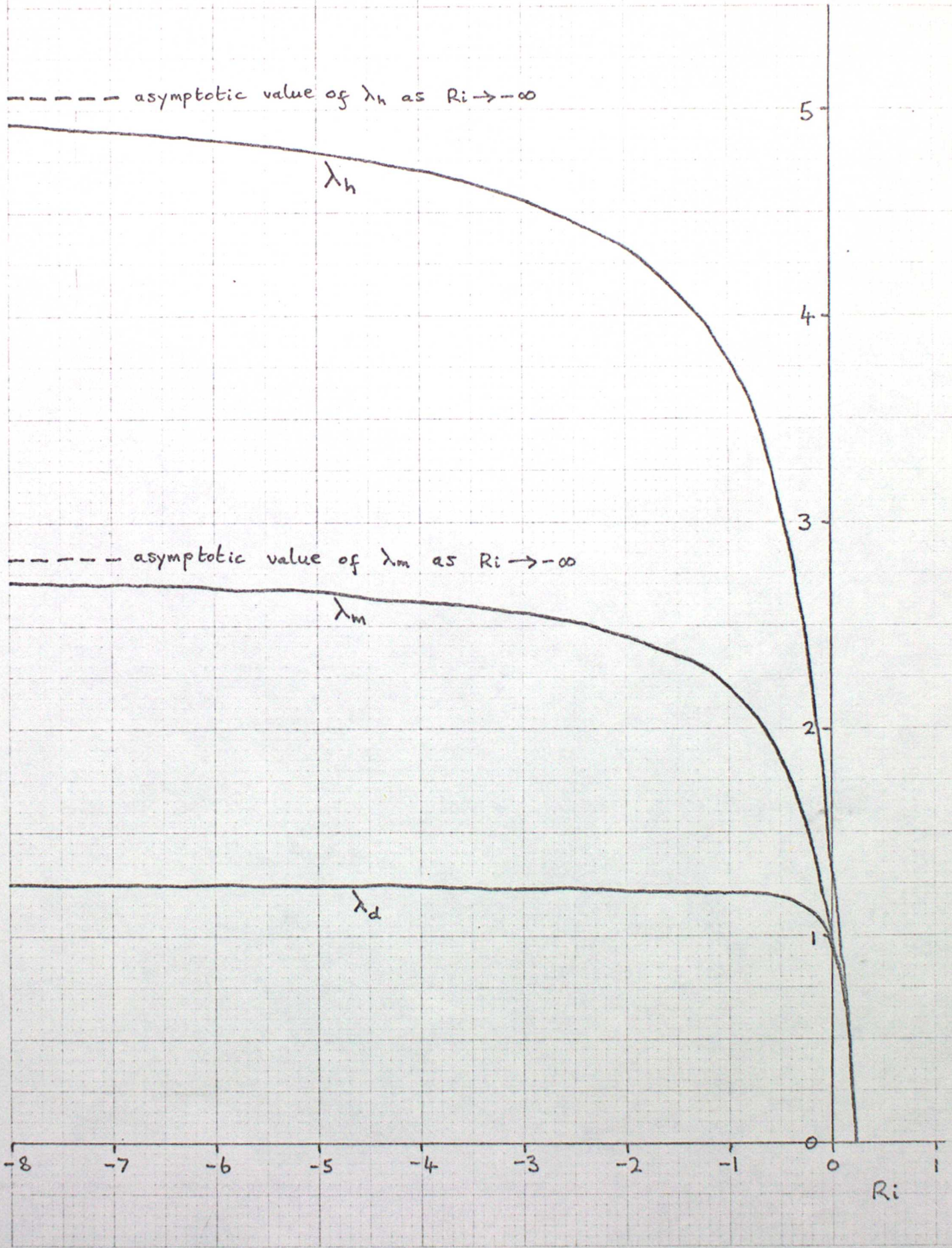

FIGURE 4.

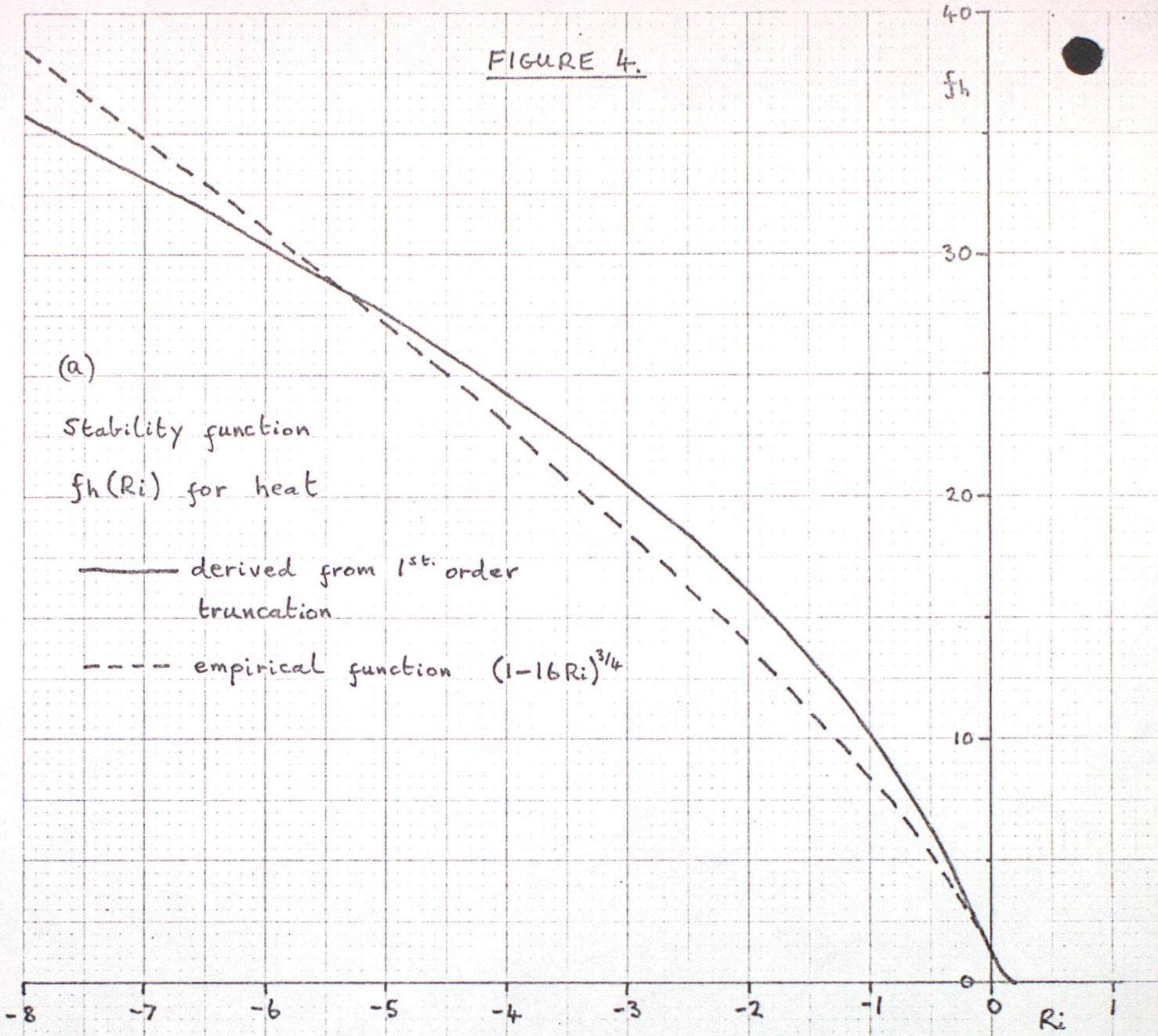

(a)

Stability function $f_h(Ri)$ for heat

——— derived from 1st. order truncation

- - - - empirical function $(1-16Ri)^{3/4}$

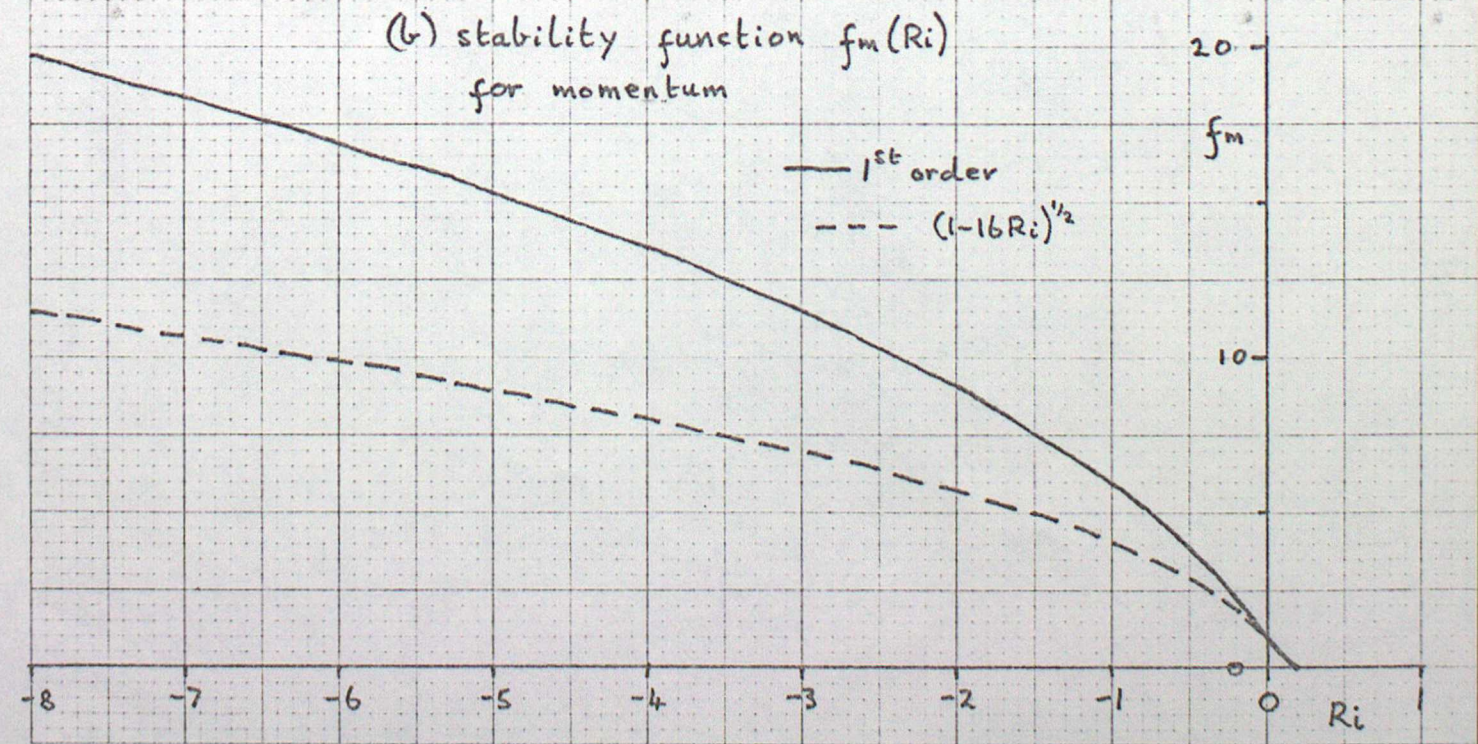

(b) stability function $f_m(Ri)$ for momentum

——— 1st order

- - - $(1-16Ri)^{1/2}$

FIGURE 5 (a)

MONIN-OBUKOV STABILITY FUNCTION FOR HEAT

——— derived from 1st. order truncation

- - - - Businger empirical function

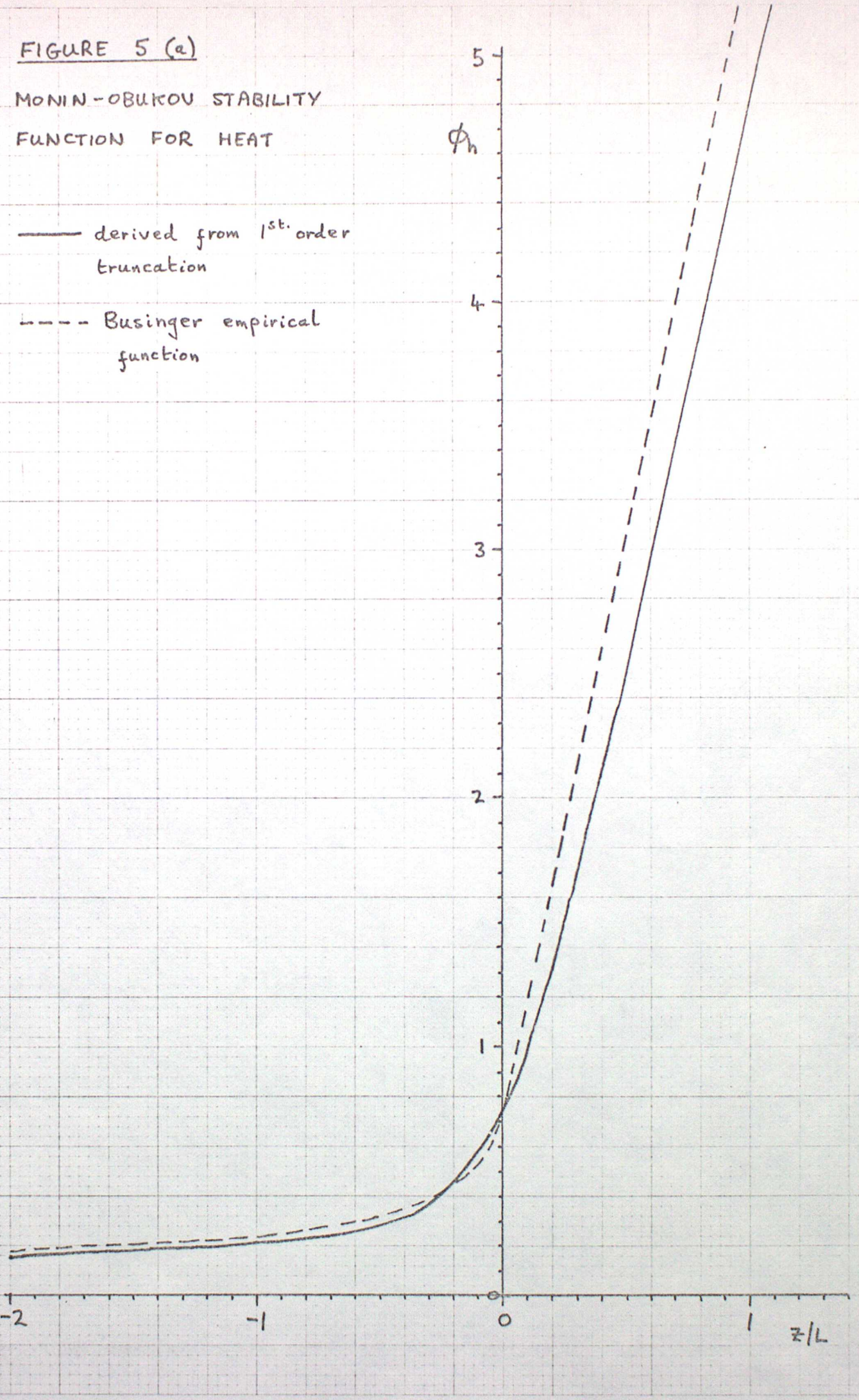

FIGURE 5(b)

MONIN-OBUKOV STABILITY FUNCTION FOR MOMENTUM

—— derived from 1st. order truncation

--- Businger empirical function

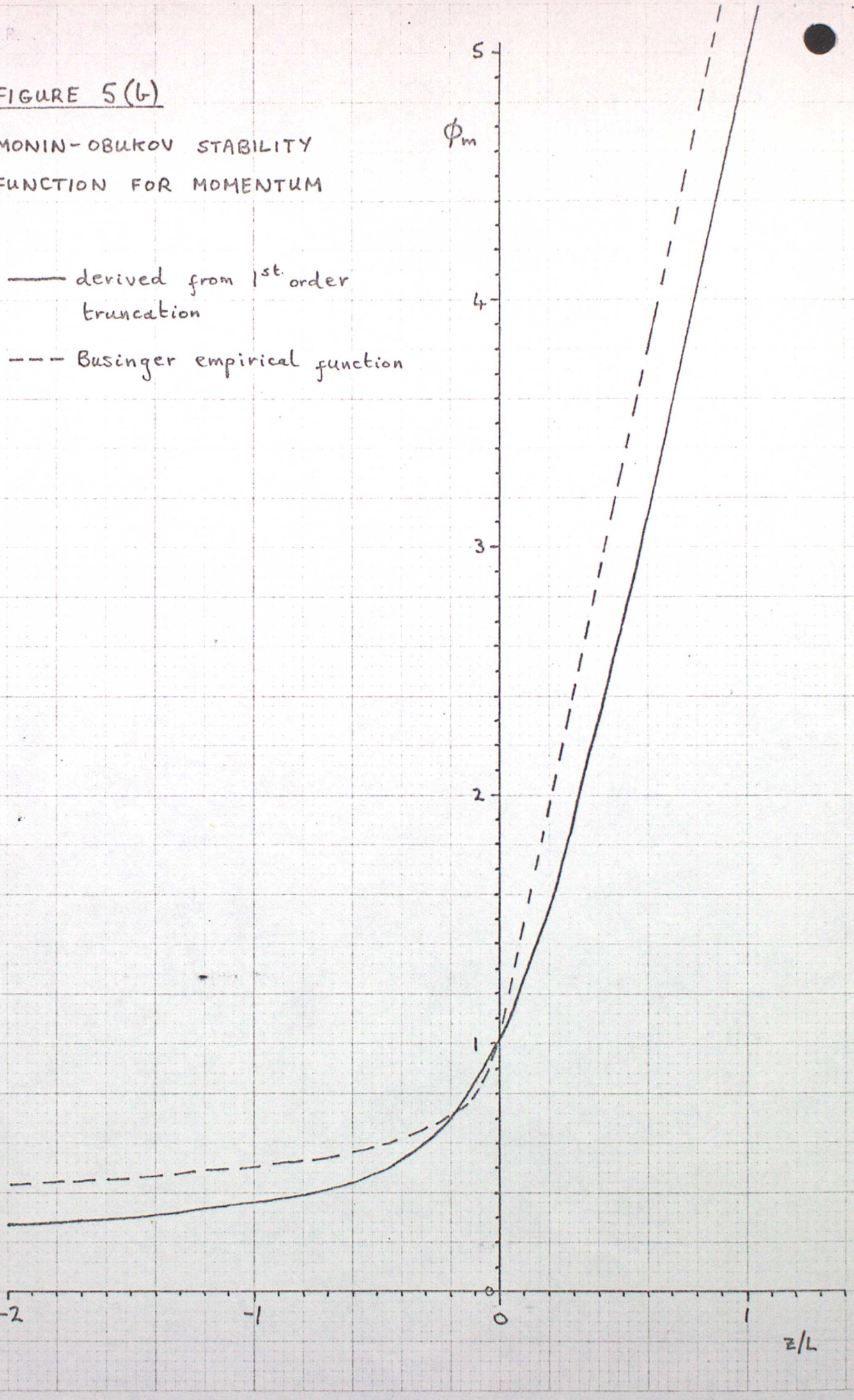

FIGURE 6.

The vertical grid and arrangement of variables.

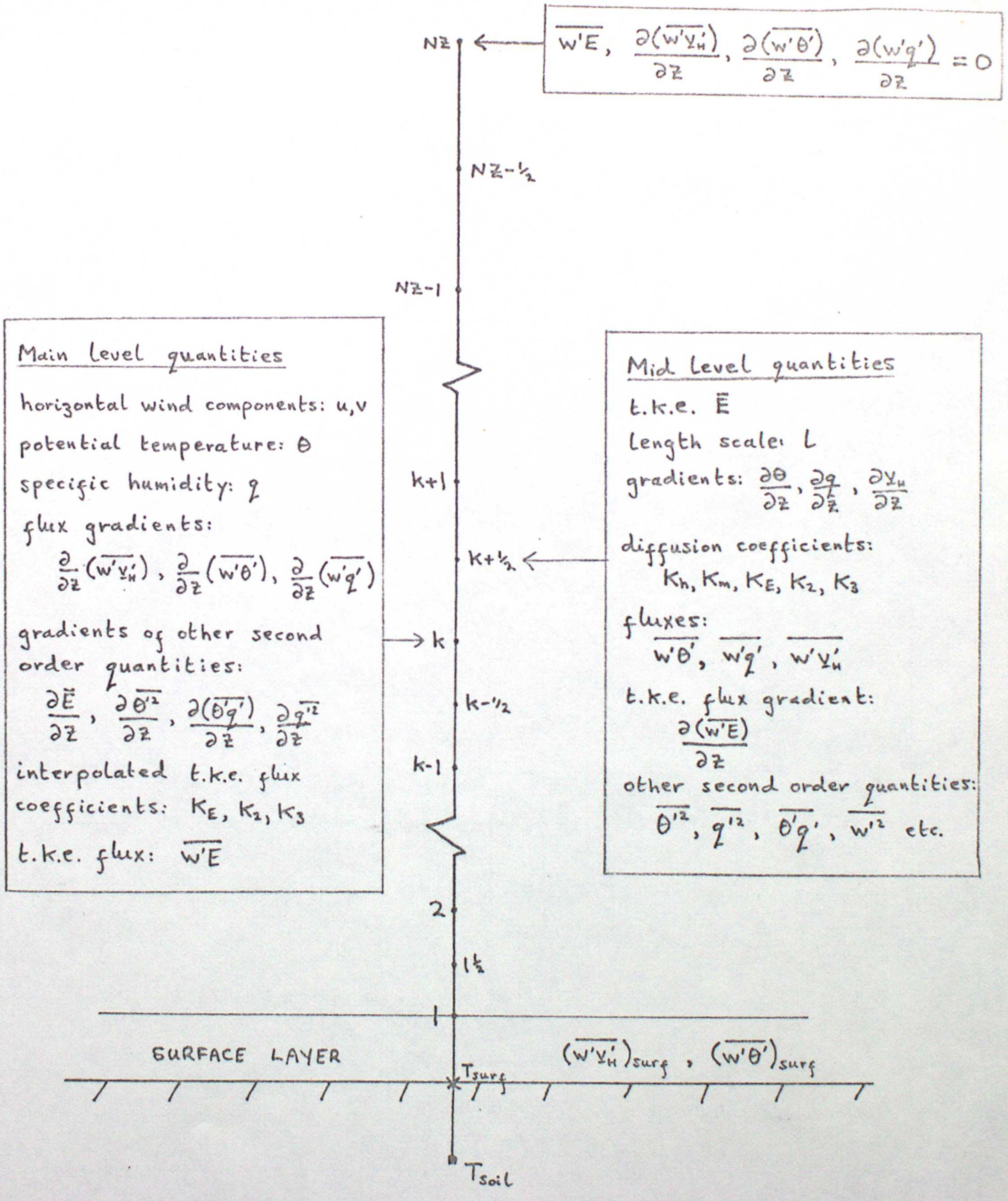

FIGURE 7.

OBSERVED PROFILES OF POTENTIAL TEMPERATURE

DURING WANGARA DAY 33.

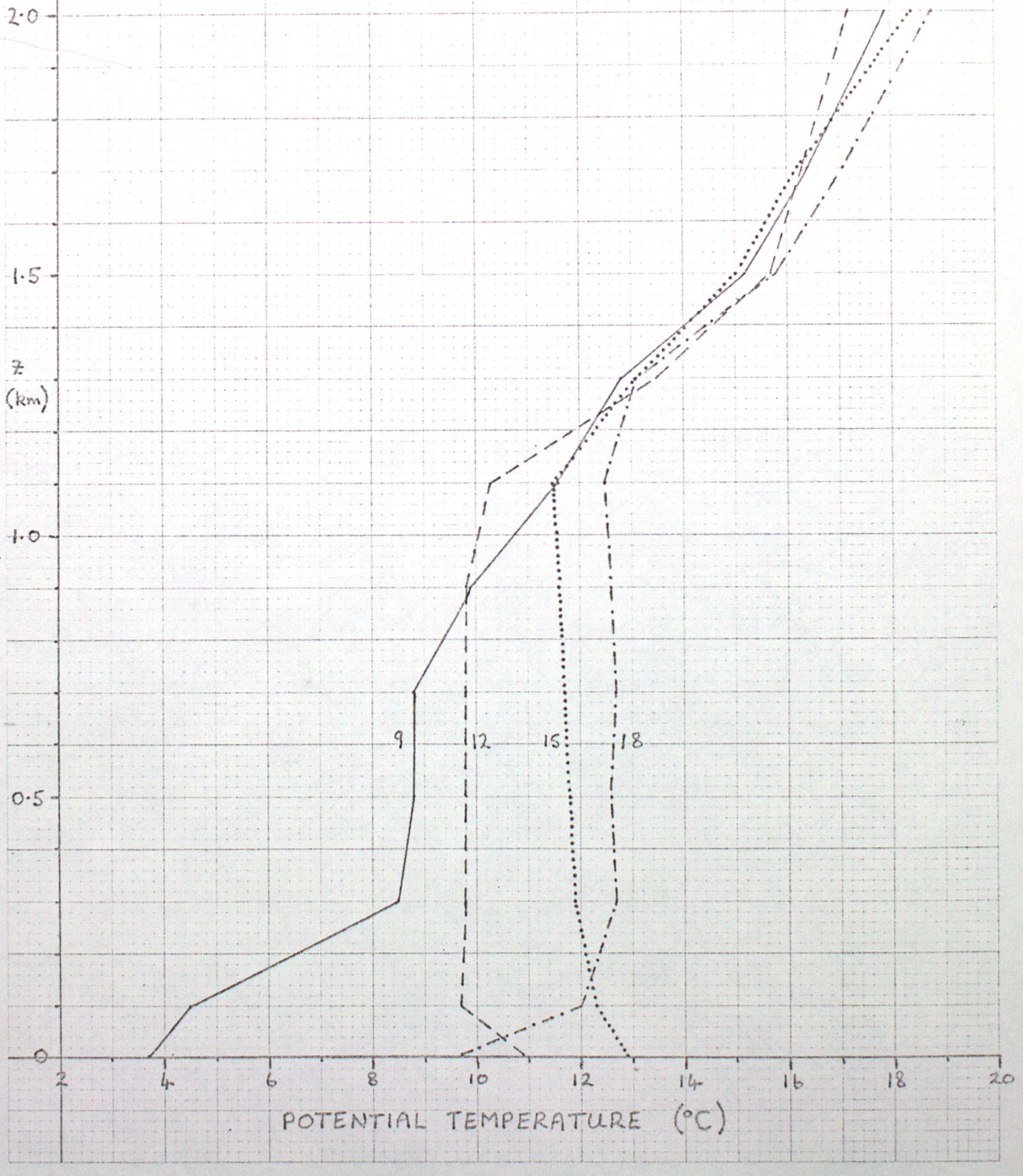

FIGURE 8.

SIMULATED PROFILES OF POTENTIAL TEMPERATURE DURING WANGARA DAY 33.

FIGURE 9.

SIMULATED AND OBSERVED SURFACE SENSIBLE HEAT FLUX AS A FUNCTION OF TIME : WANGARA d. 33

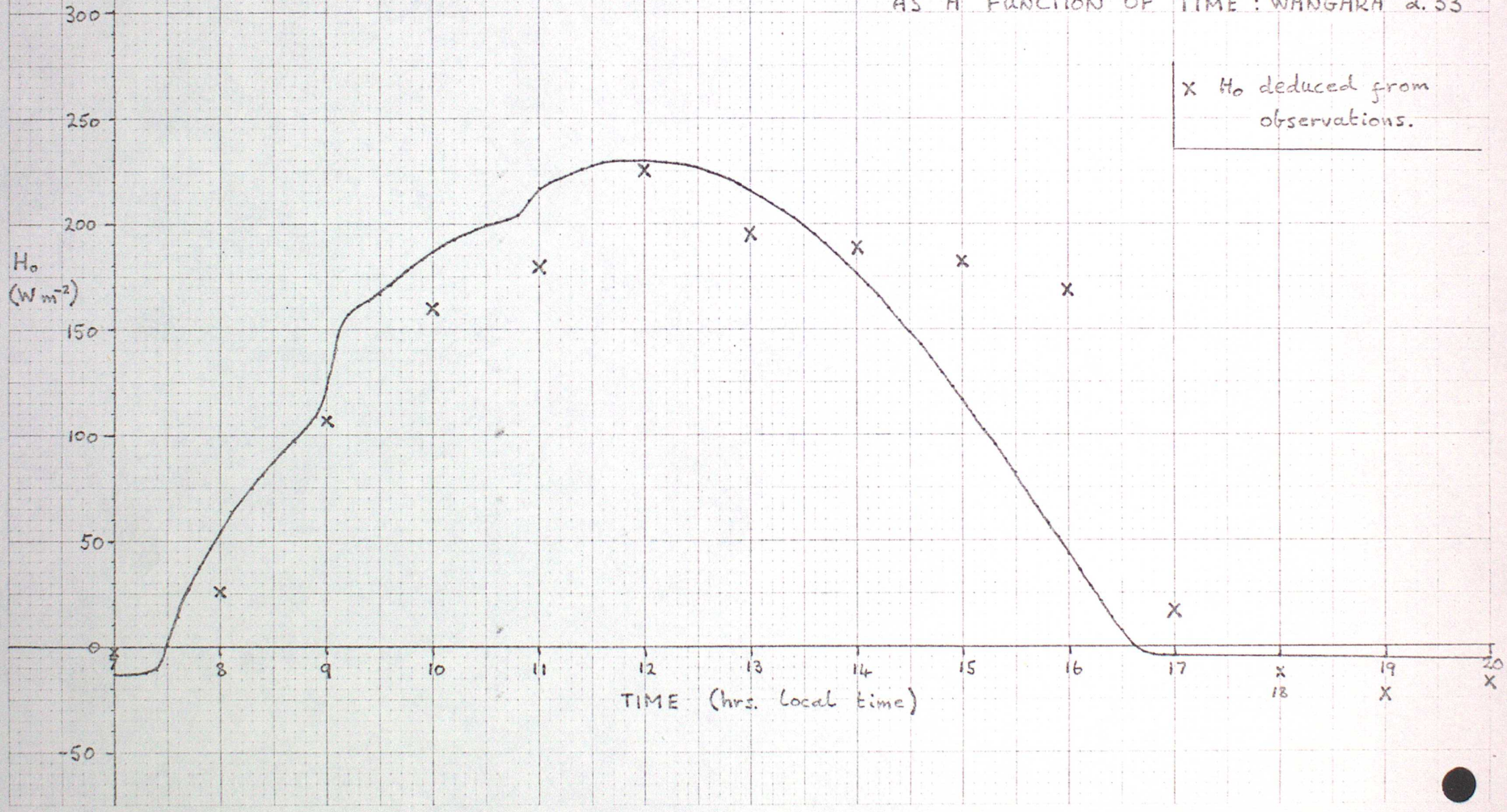

FIGURE 10.

SIMULATED BOUNDARY LAYER DEPTH AS A FUNCTION OF TIME: WANGARA DAY 33.

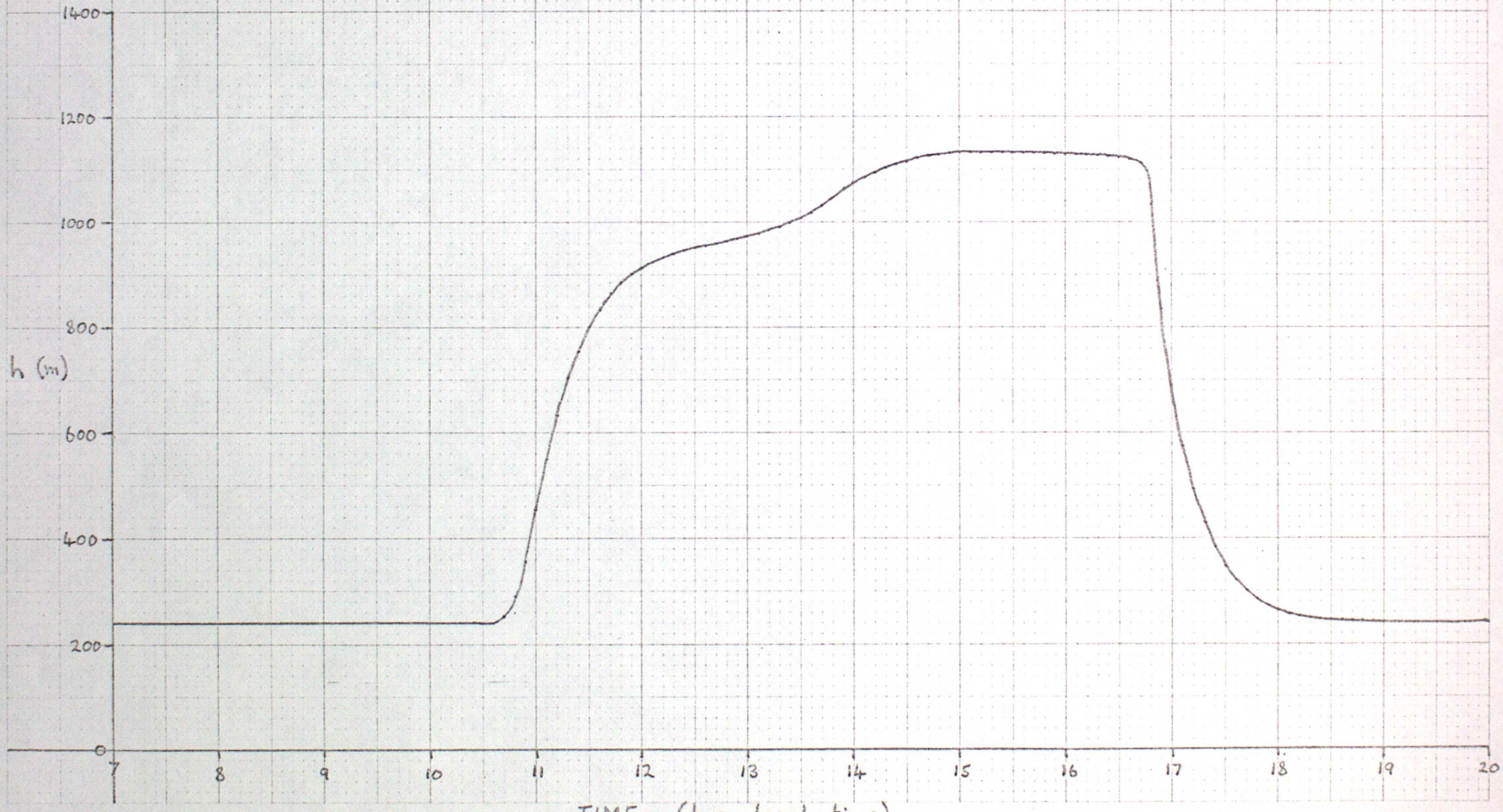

FIGURE 11.

13.00 hrs. local time

Wangara day 33 simulation.

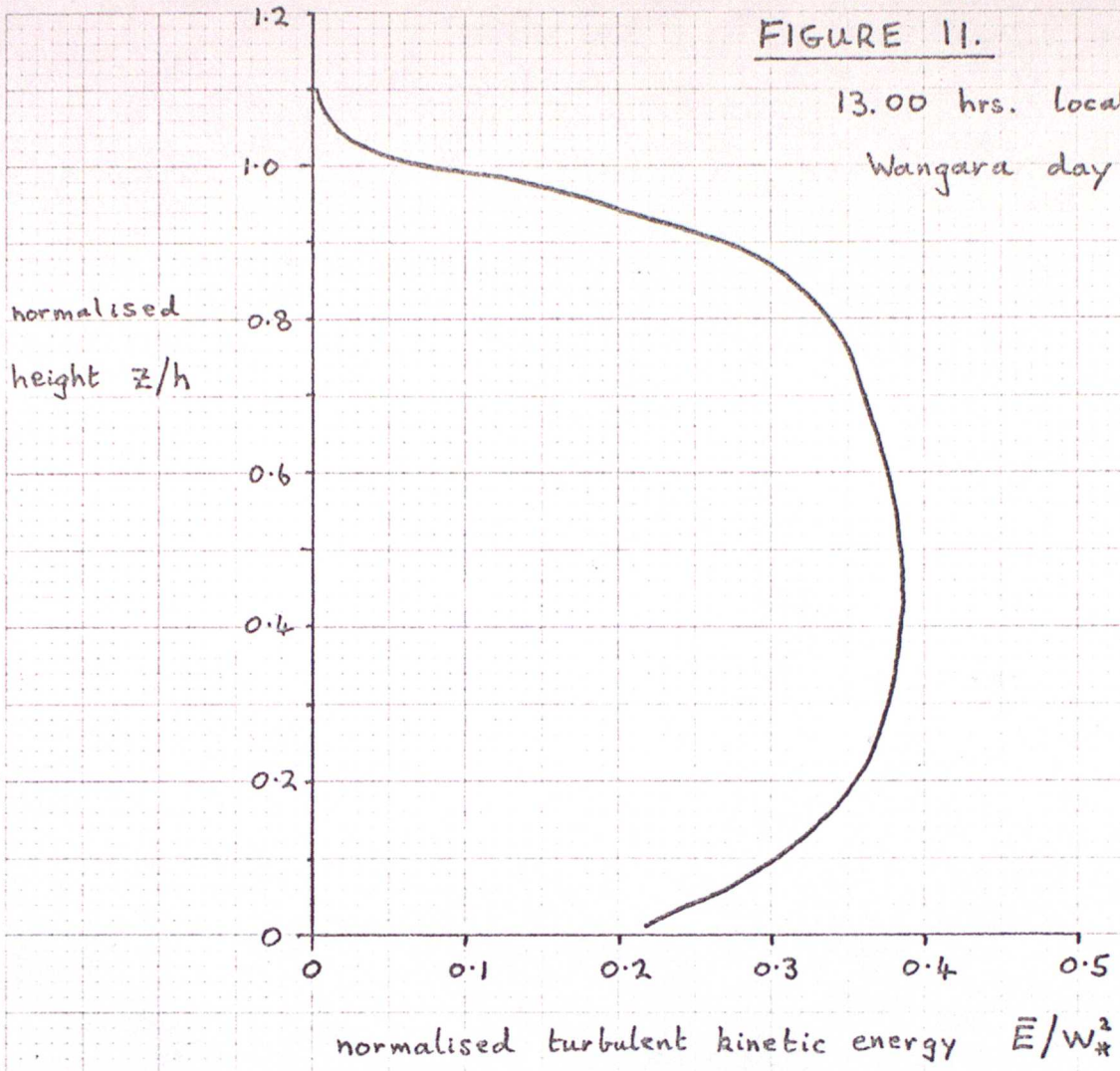

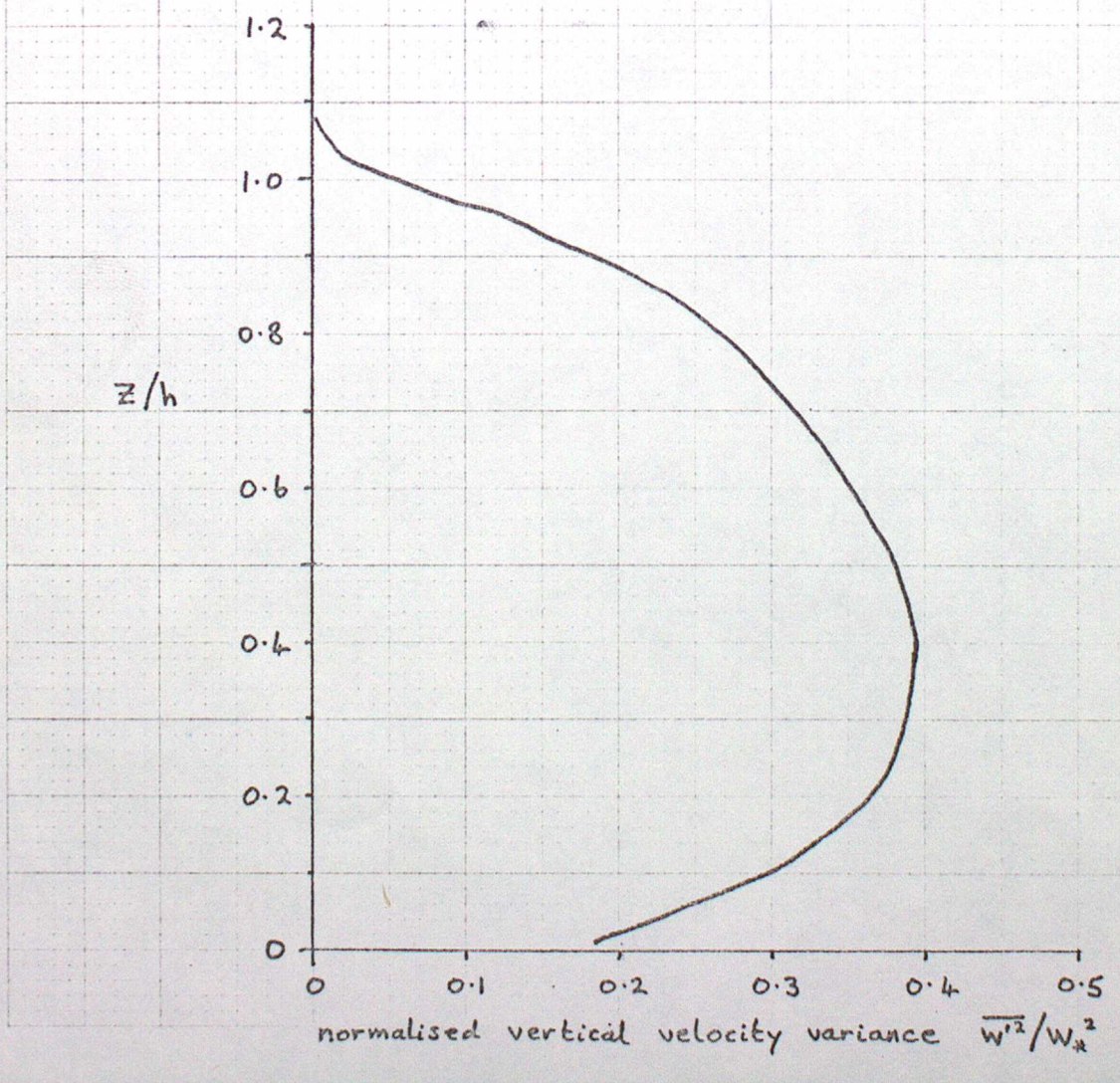

FIGURE 12.

13.00 hrs. Local time
Wangara day 33 simulation.

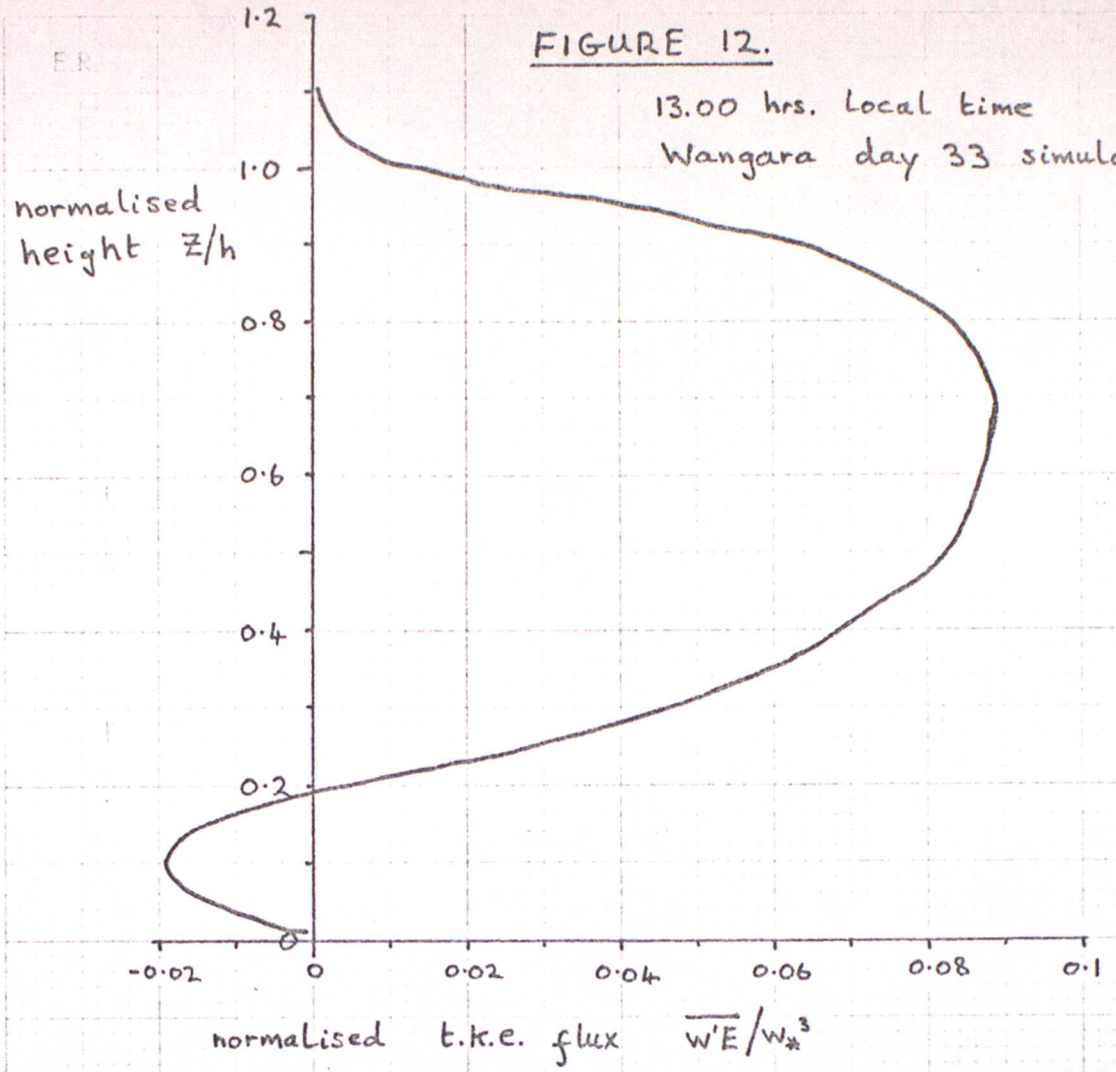

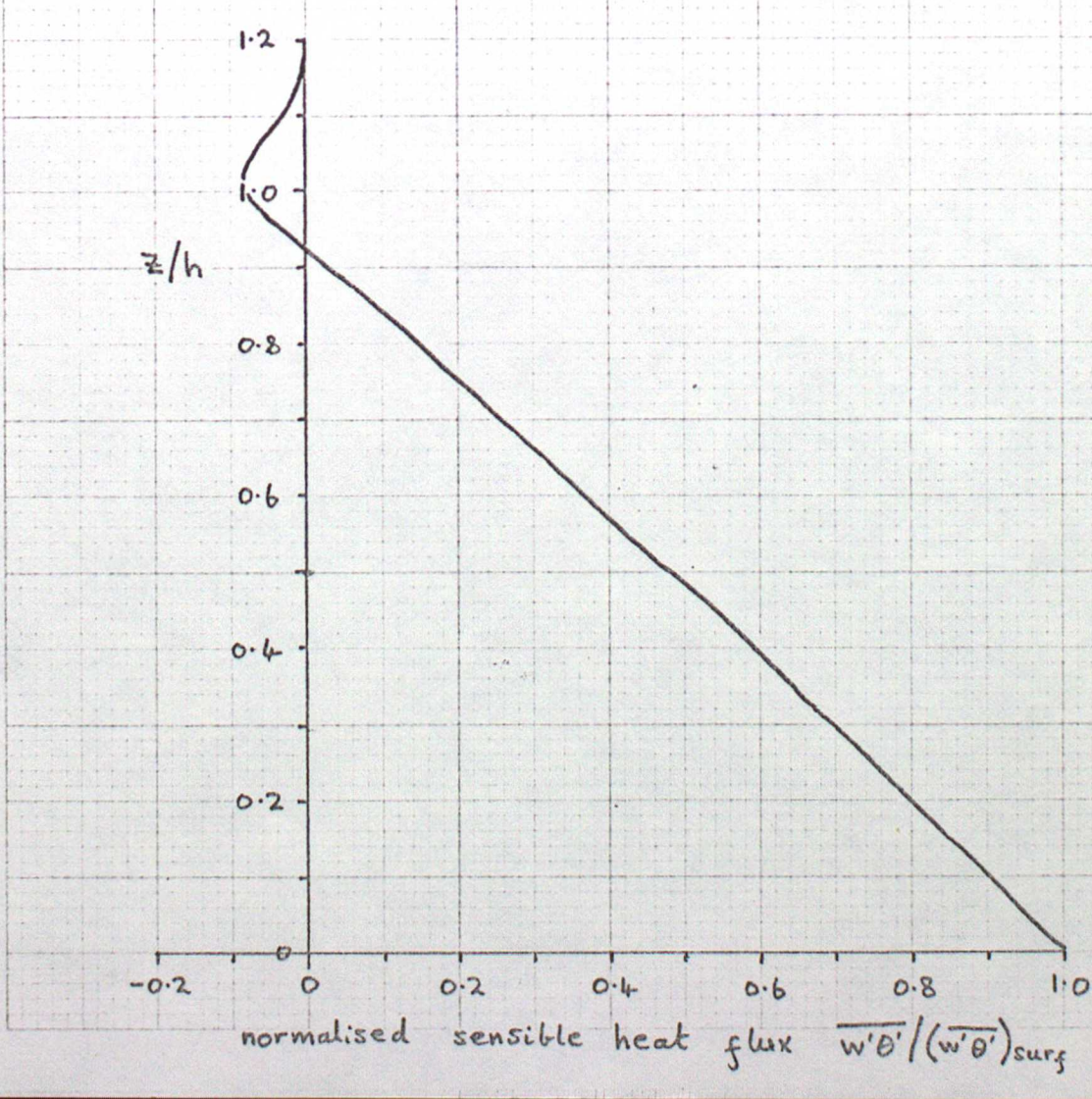

FIGURE 13.

13.00 hrs local time

Wangara day 33 simulation.

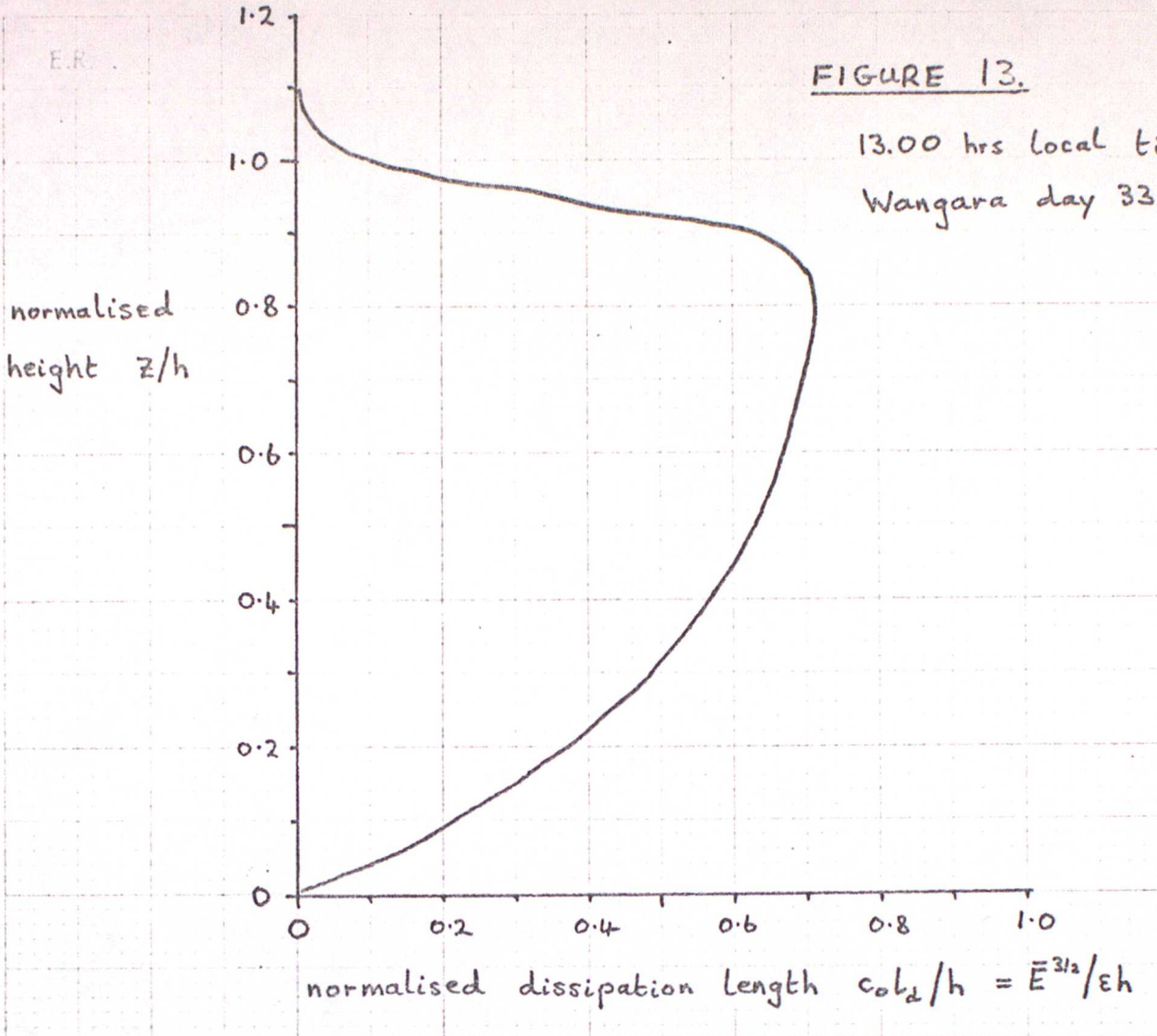

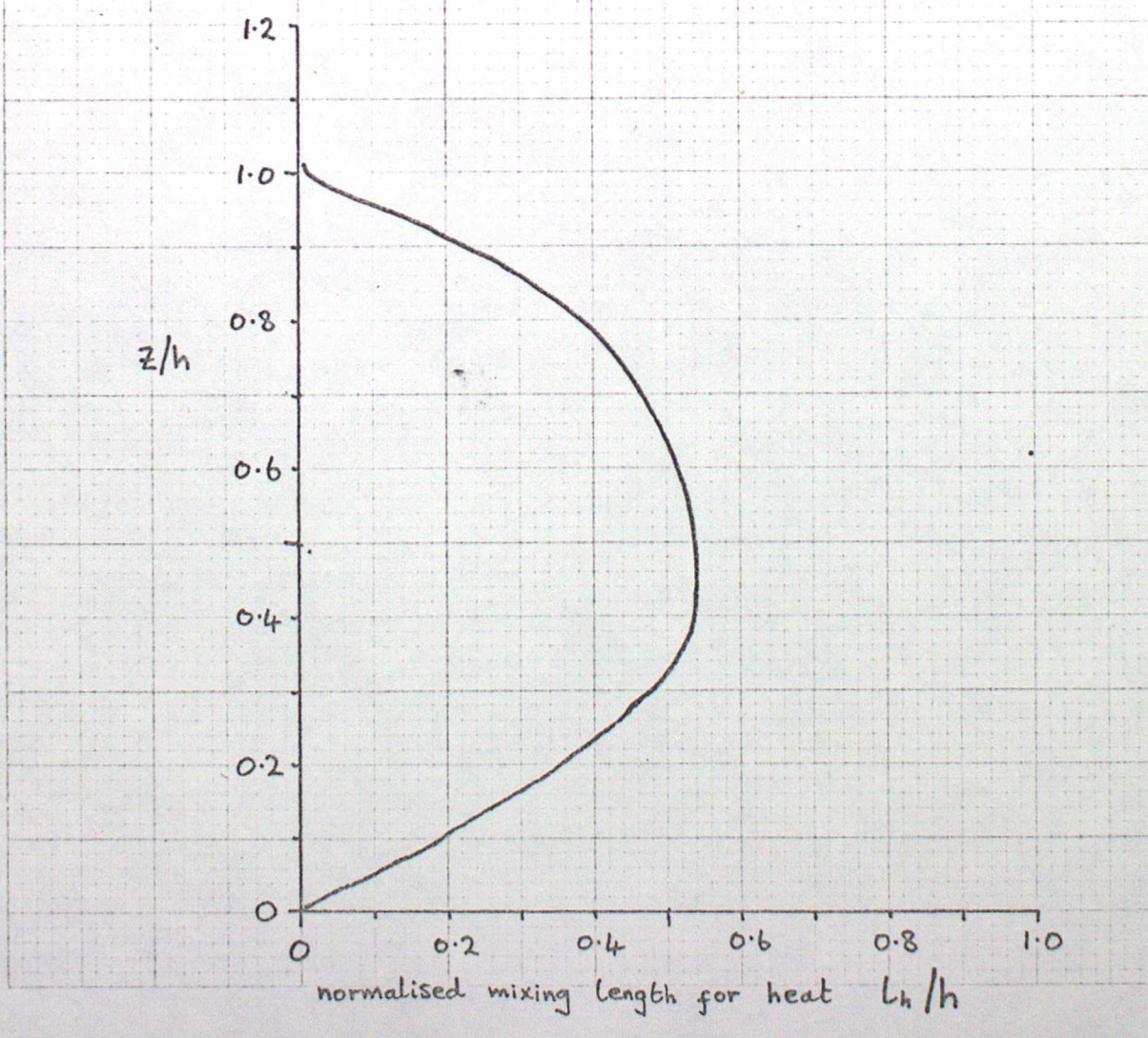

14/7/83
12.00 Z

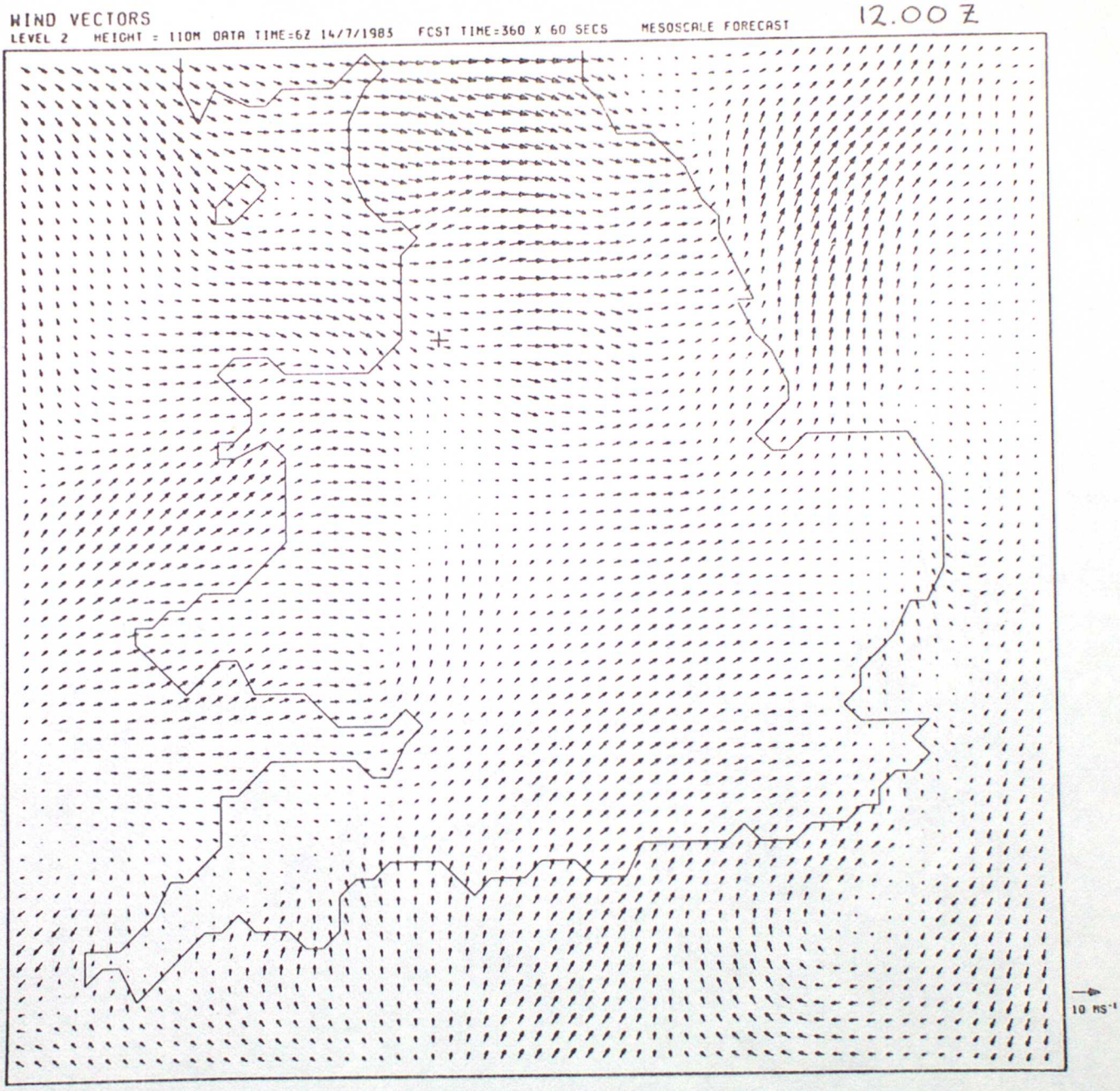

+ grid point (26,18)

FIGURE 14

14/7/83

12.00Z

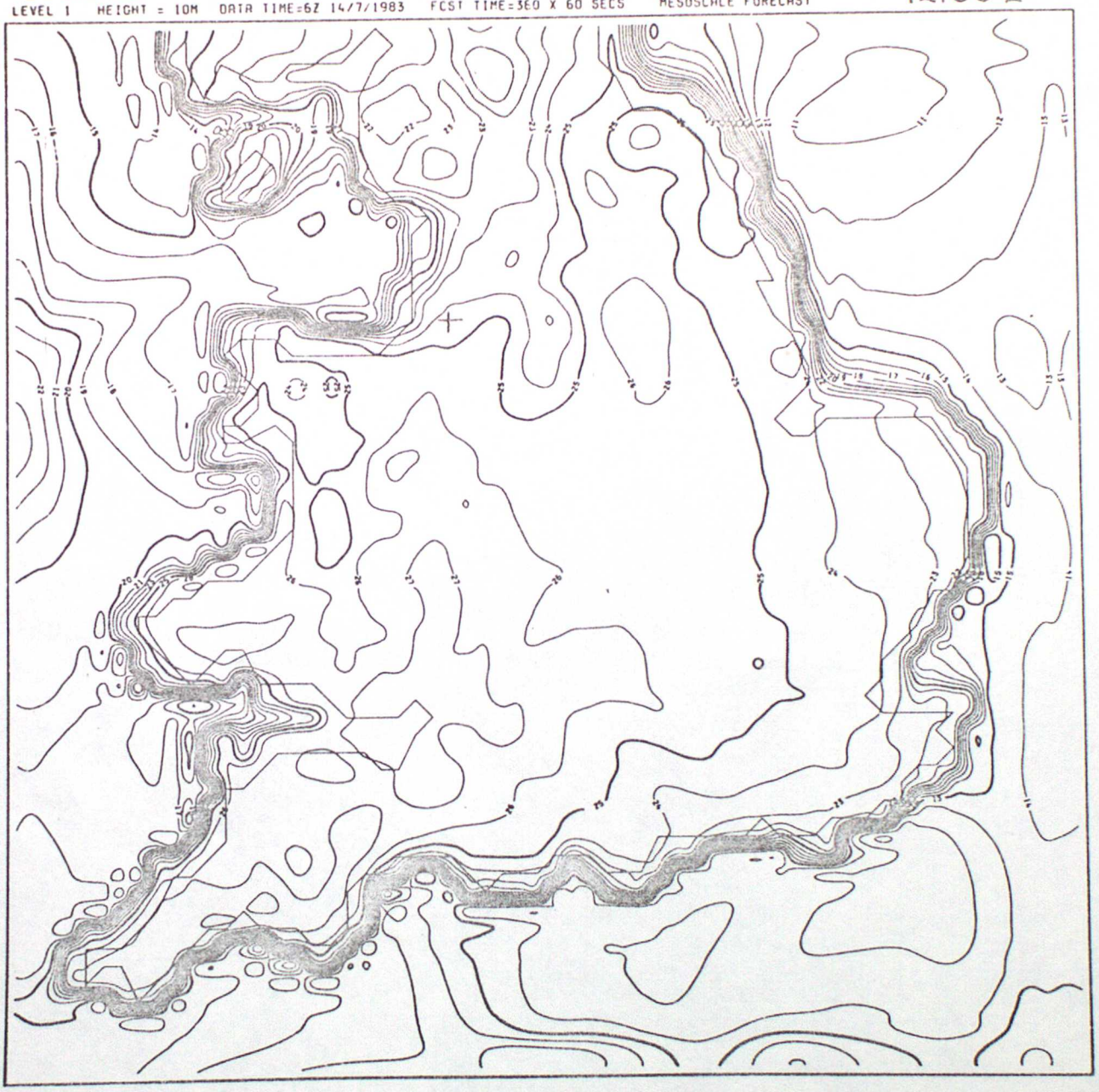

+ grid point (26,18)

FIGURE 15

14/7/83

18.00Z

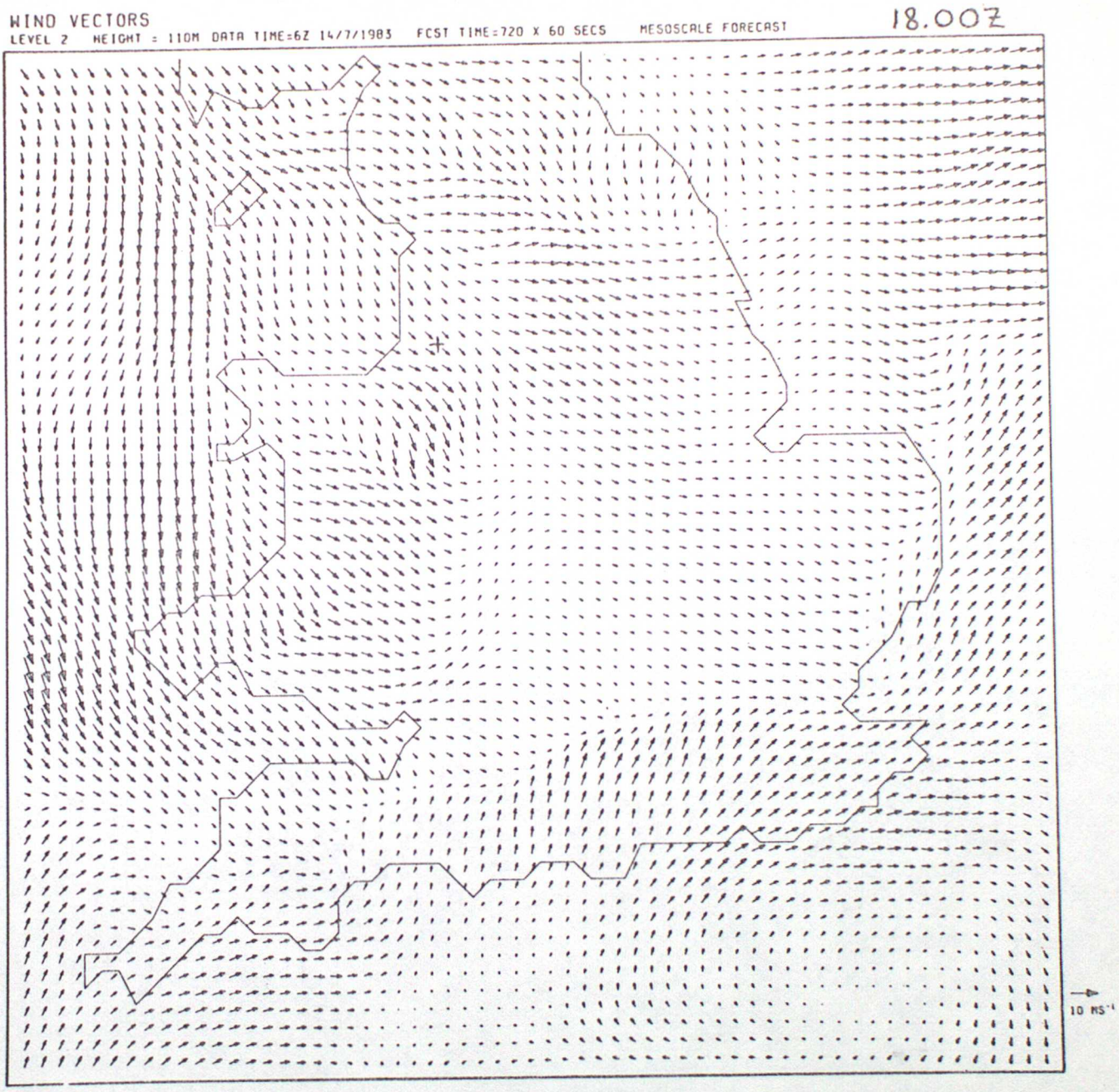

+ grid point (26,18)

FIGURE 16

14/7/83
18.00Z

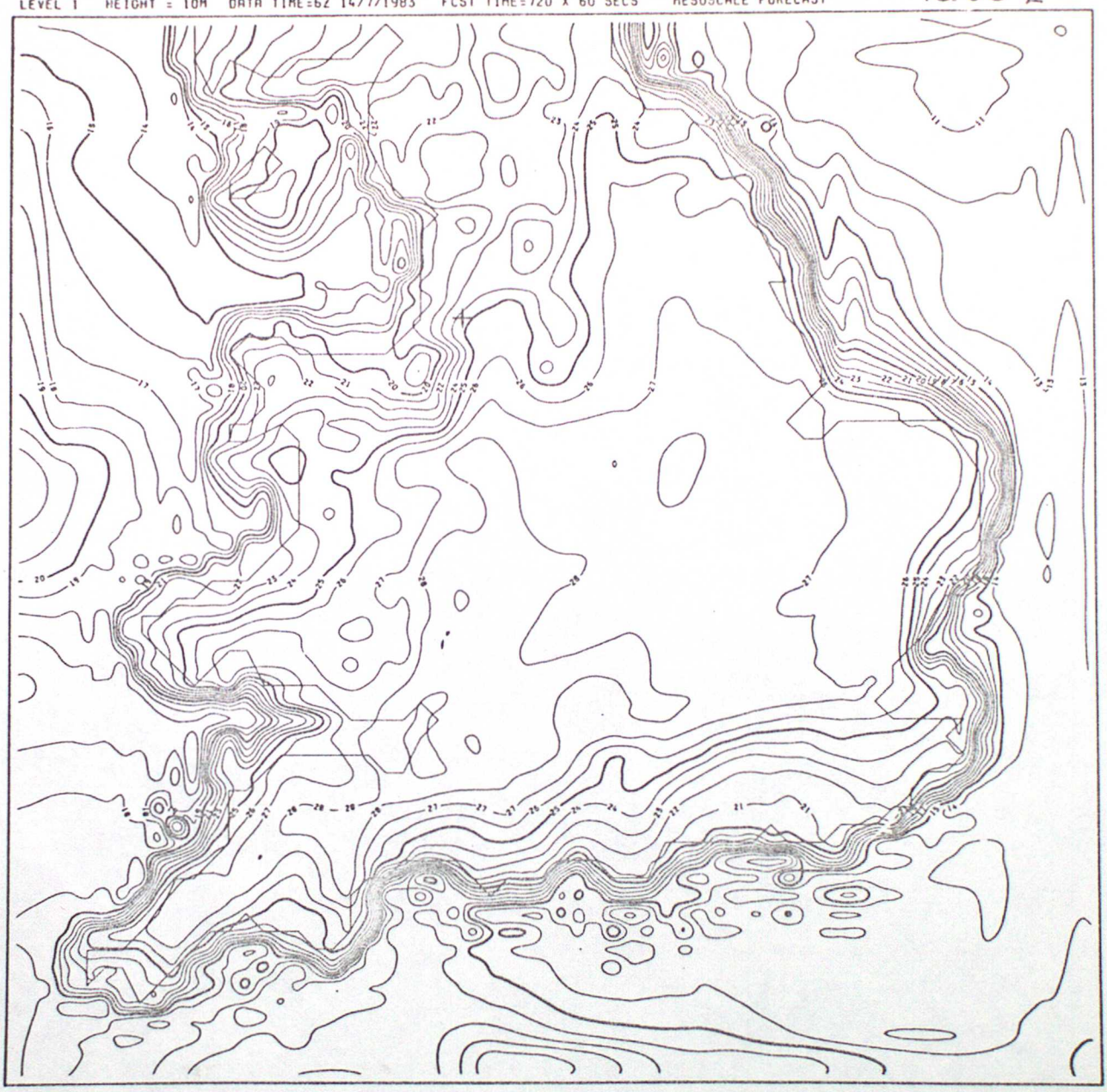

+ grid point (26,18)

FIGURE 17

14/7/83
18.00 Z

CLOUD BASE HEIGHT ISOPLETH INTERVAL = 1000 ft
DATA TIME=6Z 14/7/1983 FCST TIME=720 X 60 SECS MESOSCALE FORECAST

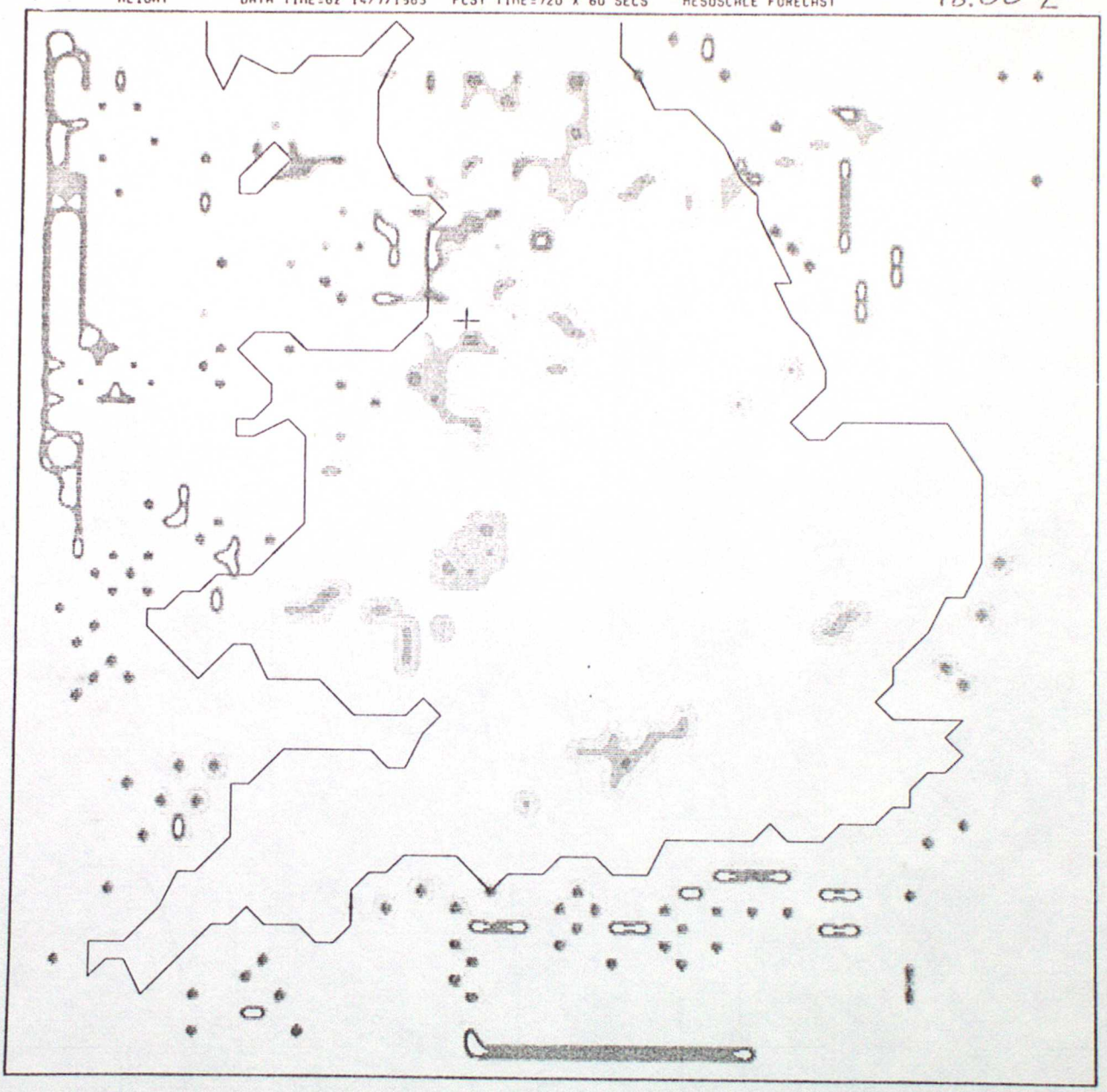

+ grid point (26, 18)

FIGURE 18

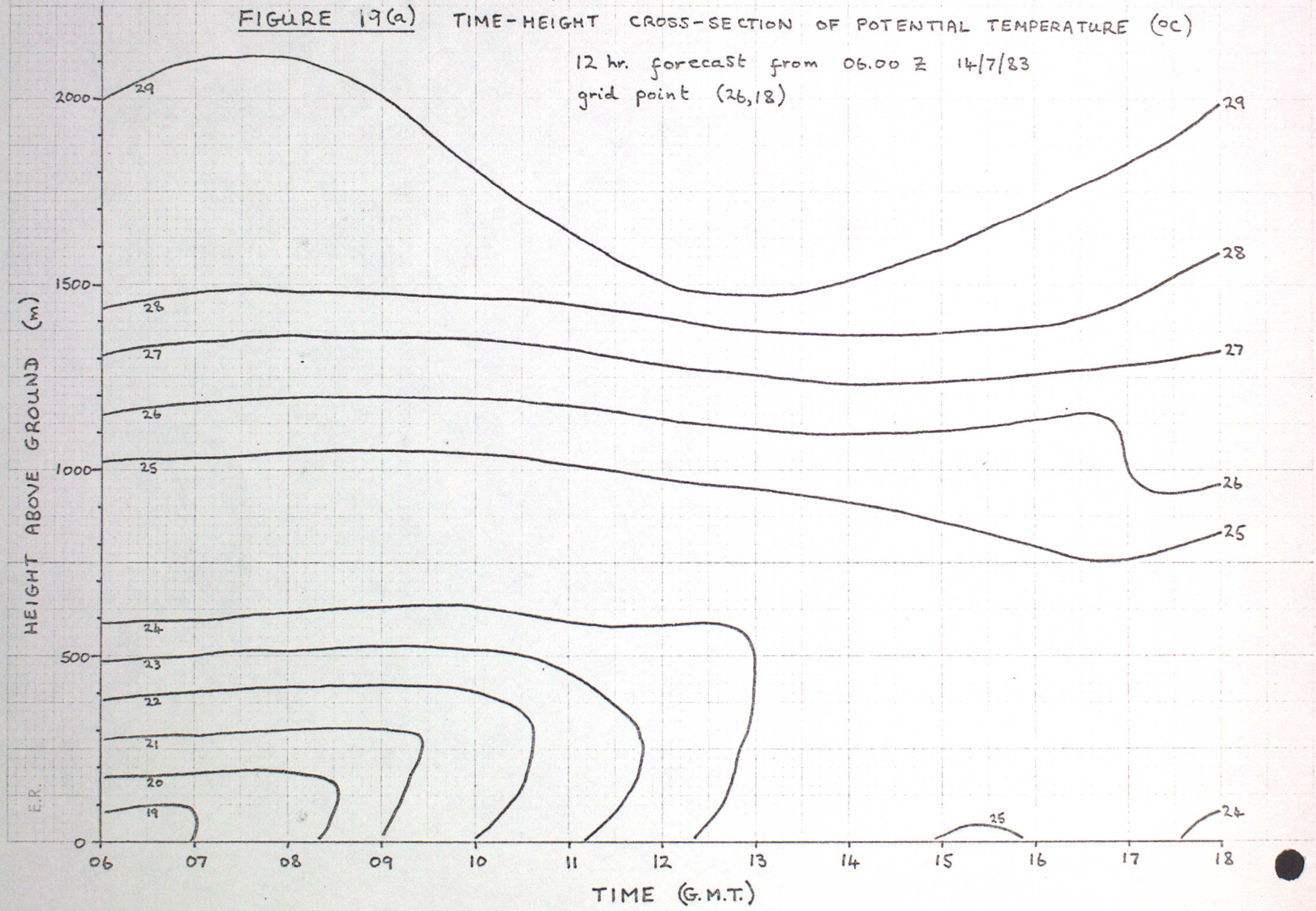
FIGURE 19(a) TIME-HEIGHT CROSS-SECTION OF POTENTIAL TEMPERATURE (°C)
12 hr. forecast from 06.00 Z 14/7/83
grid point (26,18)
HEIGHT ABOVE GROUND (m)
2000
1500
1000
500
0
29
28
27
26
25
24
23
22
21
20
19
06
07
08
09
10
11
12
13
14
15
16
17
18
TIME (G.M.T.)
E.R.

FIGURE 19(b) TIME HEIGHT CROSS-SECTION OF T.K.E. x10 ($m^2 s^{-2}$)

12 hr forecast from 06.00 Z 14/7/83

grid point (26,18)

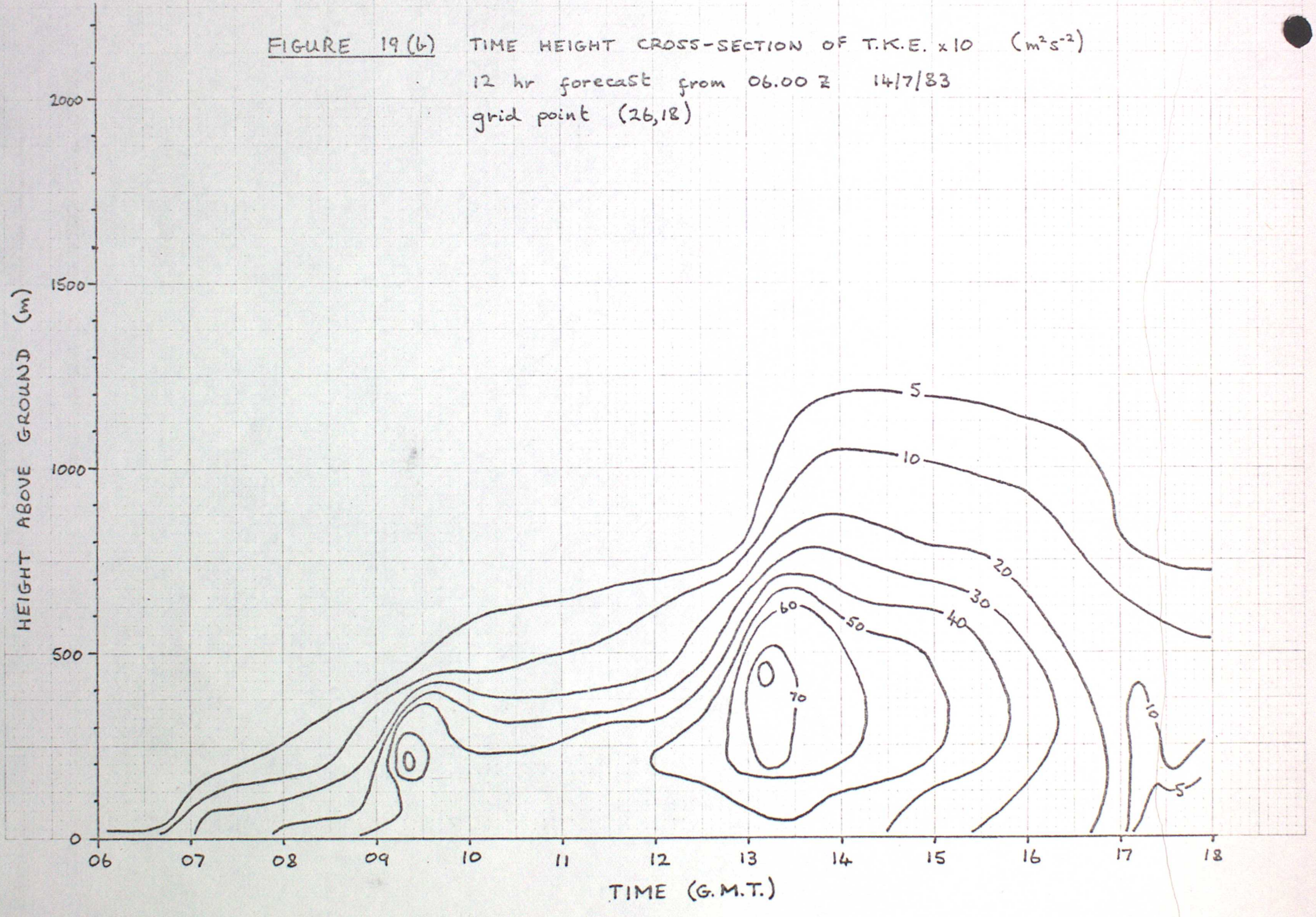

24/7/83

TEMPERATURE ISOPLETH INTERVAL = 1 DEG C

LEVEL 1 HEIGHT = 10M DATA TIME=6Z 24/7/1983 FCST TIME=0 X 60 SECS MESOSCALE FORECAST

06.00 Z

FIGURE 20.

24/7/83
12.00 Z

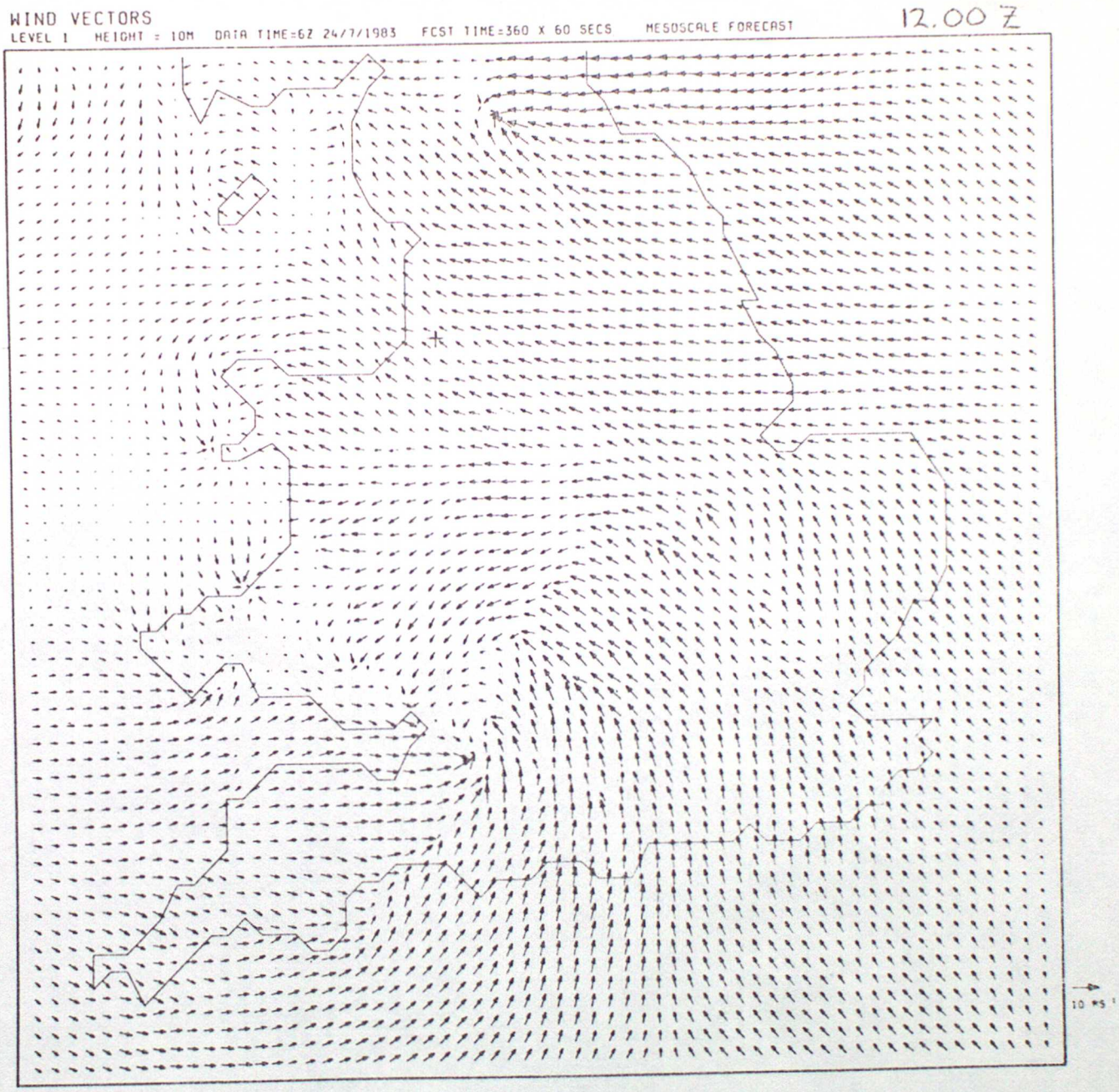

FIGURE 21.

24/7/83
12.00Z

TEMPERATURE ISOPLETH INTERVAL = 1 DEG C
LEVEL 1 HEIGHT = 10M DATA TIME=6Z 24/7/1983 FCST TIME=360 x 60 SECS MESOSCALE FORECAST

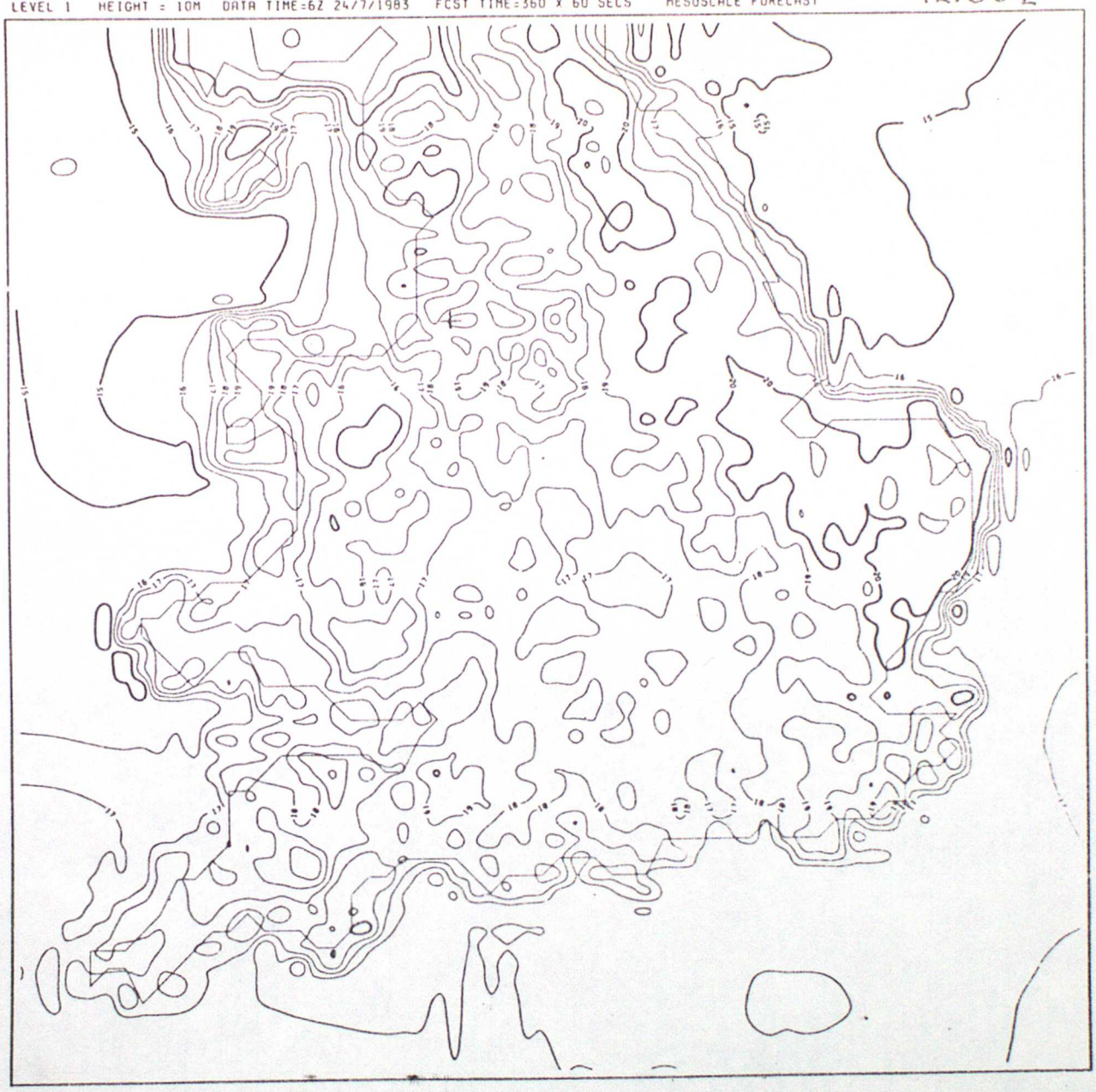

FIGURE 22.

24/7/83
12.00 Z

CLOUD BASE HEIGHT ISOPLETH INTERVAL = 1000 ft
DATA TIME=6Z 24/7/1983 FCST TIME=360 x 60 SECS MESOSCALE FORECAST

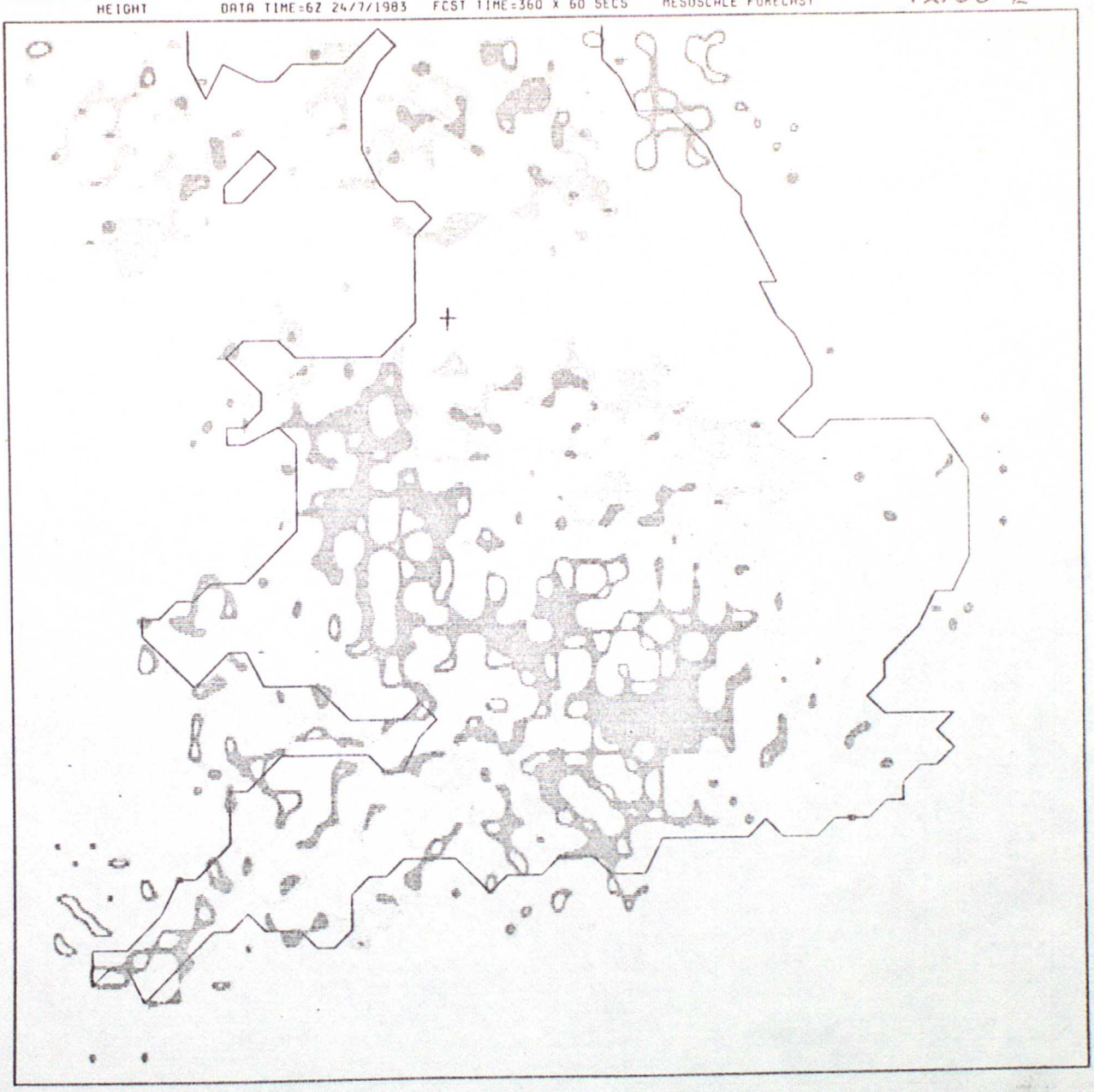

FIGURE 23.

24/7/83

18.00 Z

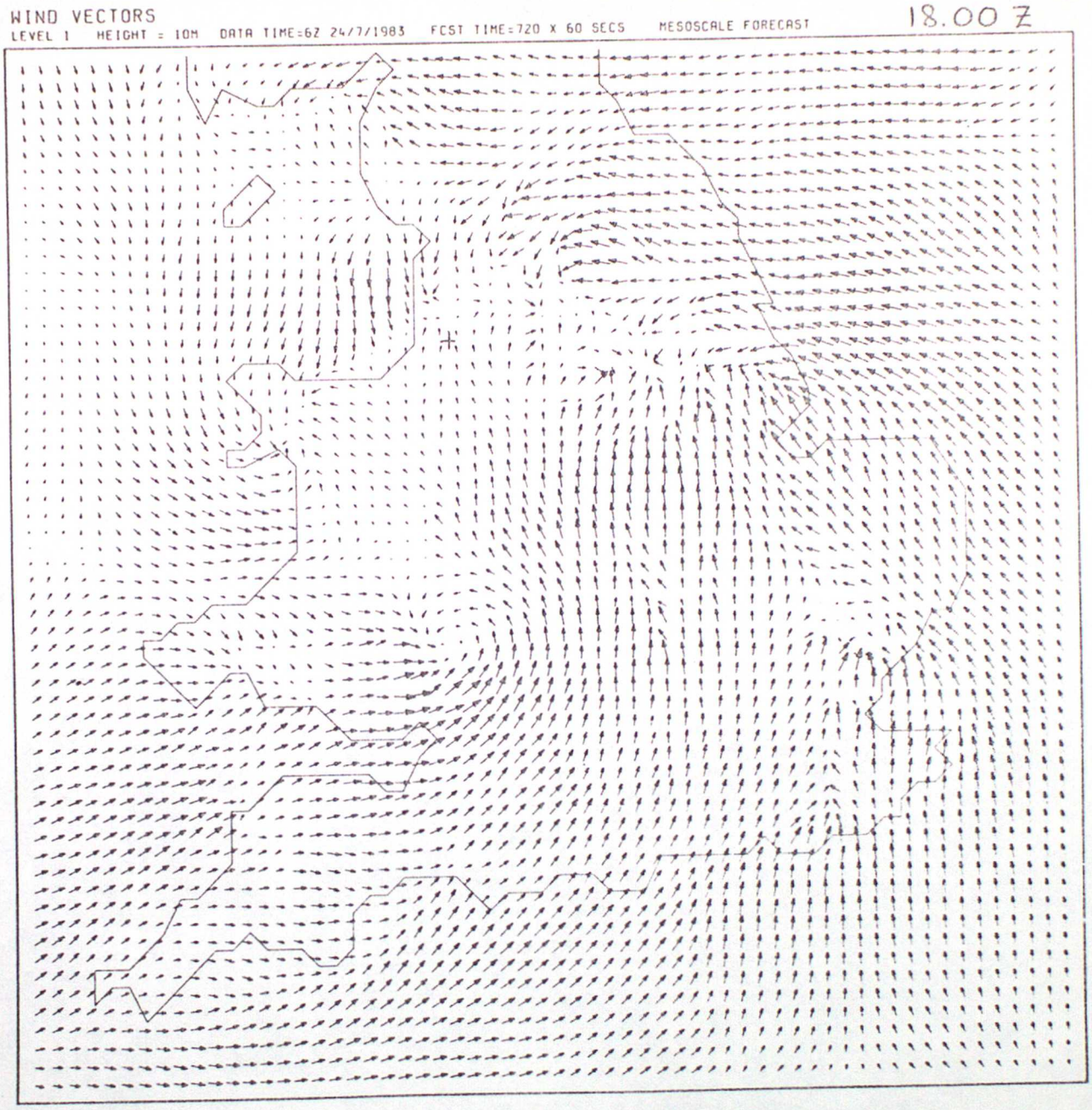

FIGURE 24.

24/7/83
18.00 Z

FIGURE 25.

24/7/83
18.00 Z

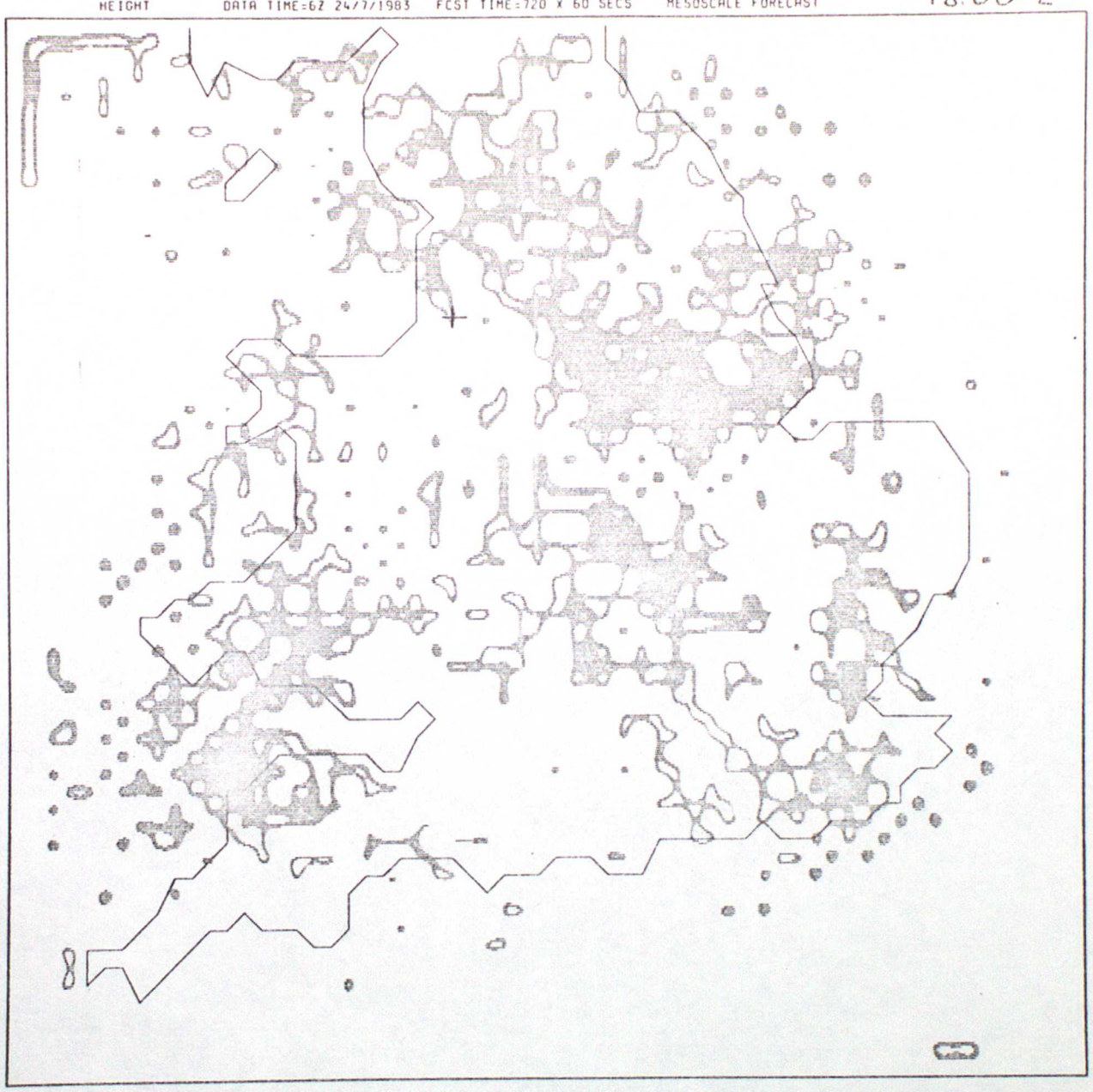

FIGURE 26.

FIGURE 27(a)

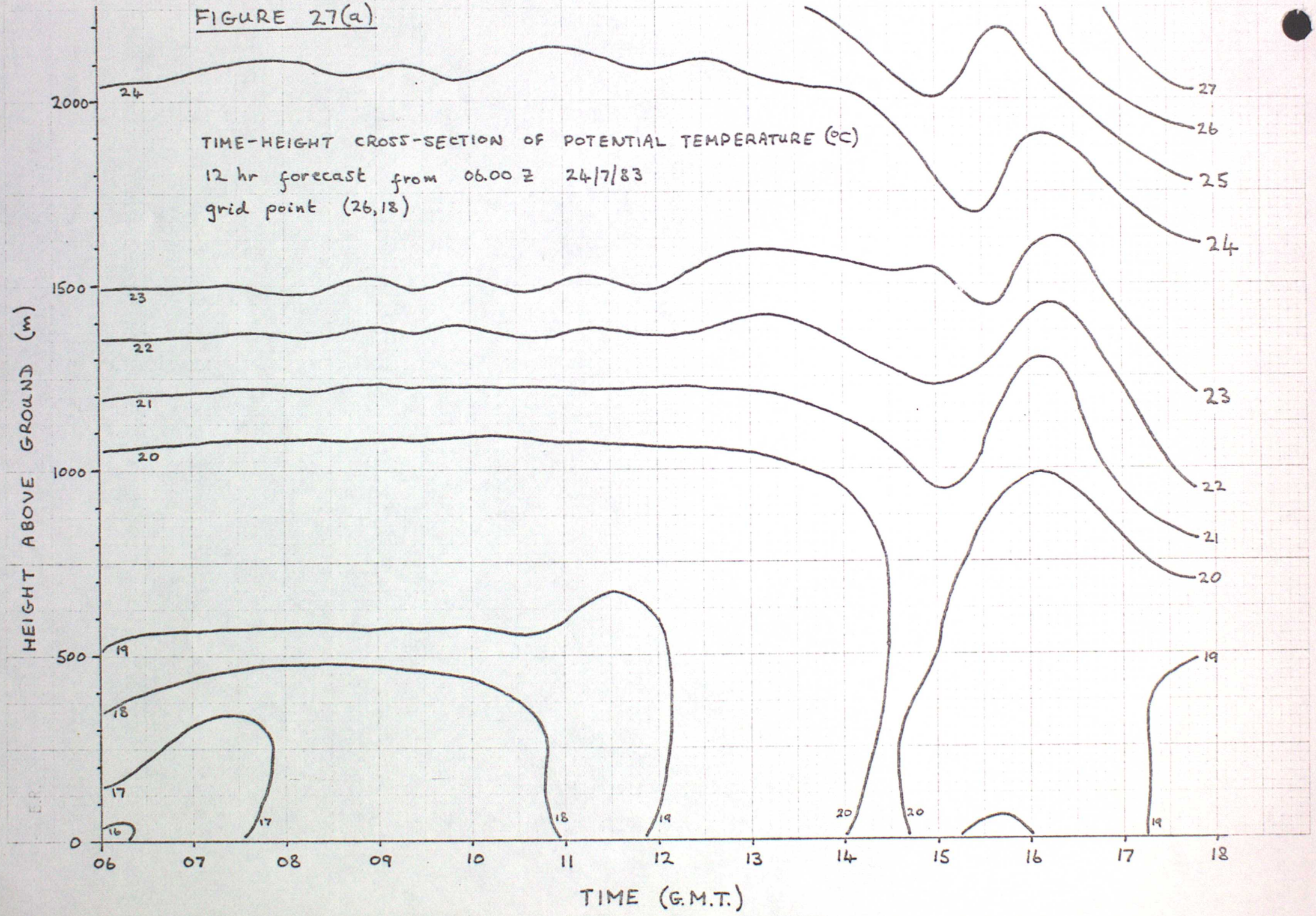
TIME-HEIGHT CROSS-SECTION OF POTENTIAL TEMPERATURE (°C)
12 hr forecast from 06.00 Z 24/7/83
grid point (26,18)
HEIGHT ABOVE GROUND (m)
2000
1500
1000
500
0
TIME (G.M.T.)
06
07
08
09
10
11
12
13
14
15
16
17
18
24
23
22
21
20
19
18
17
16
27
26
25
24
23
22
21
20
19

FIGURE 27(b) TIME-HEIGHT CROSS-SECTION OF T.K.E. x10 ($m^2 s^{-2}$)

12 hr forecast from 06.00 Z 24/7/83

grid point (26,18)